Chapter | eight

Perturbation Mitigation

All space, all time,
(The stars, the terrible perturbations of the suns,
Swelling, collapsing, ending, serving their longer, shorter use,)
Fill'd with eidolons only.

Walt Whitman (1819–1892)

In the first part of this chapter we show how to adjust or constrain some of the initial conditions to reduce the amount of fuel required to counter the undesirable effects resulting from the J_2 perturbation. In contrast to most of the previous developments, which have used the relative position in the rotating reference frame, the current development utilizes Hamiltonian mechanics, discussed in Chapter 3, and is based on Brouwer's theory [66] introduced in Section 3.4. The first-order analysis is extended to the second-order in the Yan–Alfriend theory. A comparison of several linear and nonlinear analytical relative motion propagation theories is presented on the basis of a *nonlinearity error index*, which is a measure of the relative importance of modeling geometric nonlinearity, eccentricity, and J_2 as a function of the formation size.

The second part of the chapter deals with the perturbations in the fundamental in-plane and cross-track frequencies due to J_2. We also present an intelligent scheme for formation maintenance and inter-satellite fuel balancing, which accommodates a significant portion of the perturbations rather than countering them with thrust.

8.1 DYNAMIC CONSTRAINTS FOR J_2 MITIGATION

The attractive solutions of the CW or Tschauner–Hempel–Lawden equations derived in Chapter 5, obtained under the assumption of a spherical Earth, get disturbed in the presence of gravitational perturbations, as shown in Chapter 7. In particular, differences in the mean semimajor axis, eccentricity and inclination cause along-track, radial, and cross-track drift. In addition, perigee rotation causes in-plane and cross-track frequencies to no longer be equal. This means, depending on the desired formation, that control may be required to maintain the formation. For example, as shown in Section 2.6, if the chief is in a 7100 km circular orbit with $i = 70°$, the Δv required to counter the differential nodal

Spacecraft Formation Flying; ISBN: 9780750685337

precession for a relative motion orbit that has a maximum cross-track displacement of 1 km caused by an inclination difference is approximately 41 m/s/yr. This estimate is based on the assumption that the corrections are impulsive and are performed once per orbit. In addition, the fuel requirements for countering along-track drift and perigee rotation effects can be prohibitive, depending on the reference orbit and size of the formation.

We note that if the momenta of the satellites in a formation are equal then the angle rates are equal and the satellites will not drift apart. If the momenta are not equal then, in general, some of the angle rates will not be equal, and the two satellites will drift apart. The development in this section focuses on how to select the initial momenta to minimize this drift.

The dimensionless averaged Hamiltonian, Eqs. (3.19) and (3.20), provide the dimensionless angle rates

$$\dot{l} = \frac{\partial \bar{\mathcal{H}}}{\partial L} = \frac{1}{L^3} + \epsilon \left(\frac{3}{4L^7}\right)\left(\frac{L}{G}\right)^3 \left(1 - 3\frac{H^2}{G^2}\right) \tag{8.1}$$

$$\dot{g} = \frac{\partial \bar{\mathcal{H}}}{\partial G} = \epsilon \frac{3}{4L^7}\left(\frac{L}{G}\right)^4 \left(1 - 5\frac{H^2}{G^2}\right) \tag{8.2}$$

$$\dot{h} = \frac{\partial \bar{\mathcal{H}}}{\partial H} = \epsilon \frac{3}{2L^7}\left(\frac{L}{G}\right)^4 \left(\frac{H}{G}\right) \tag{8.3}$$

Note that $\varepsilon = -J_2$. It is advantageous now to transform from the generalized momenta (L, G, H) to the orbital elements (a, η, i). Using Eqs. (8.1)–(8.3) the angle rates become

$$\dot{l} = \frac{1}{a^{3/2}} + \epsilon \left(\frac{3}{4a^{7/2}\eta^3}\right)\left(1 - 3\cos^2 i\right) \tag{8.4}$$

$$\dot{g} = \epsilon \left(\frac{3}{4a^{7/2}\eta^4}\right)\left(1 - 5\cos^2 i\right) \tag{8.5}$$

$$\dot{h} = \epsilon \left(\frac{3}{2a^{7/2}\eta^4}\right)\cos i \tag{8.6}$$

It can be shown from Eqs. (8.1) and (8.2) that the mean argument of latitude rate is

$$\dot{\lambda} = \dot{l} + \dot{g} = \frac{1}{a^{3/2}} + \epsilon \left(\frac{3}{4a^{7/2}\eta^4}\right)\left[\eta\left(1 - 3\cos^2 i\right) + \left(1 - 5\cos^2 i\right)\right] \tag{8.7}$$

Any two satellites in a formation will drift apart if the difference in any of their respective angle rates is not zero, i.e., if $\delta\dot{\lambda} = \left(\dot{\lambda}_2 - \dot{\lambda}_1\right) \neq 0$, or $\delta\dot{g} = (\dot{g}_2 - \dot{g}_1) \neq 0$, or $\delta\dot{h} = \left(\dot{h}_2 - \dot{h}_1\right) \neq 0$. Cross-track drift is determined by $\delta\dot{h} = 0$ and the radial drift is determined primarily by $\delta\dot{g}$. As discussed in Section 7.1 and also in Ref. [143], the in-plane or along-track drift is determined by $\left(\delta\dot{\lambda} + \delta\dot{h}\cos i\right)$.

Expanding the three angle rate equations, Eqs. (8.7), (8.5), and (8.6), into a Taylor series about the reference or chief satellite orbit, denoted by the subscript "0", and retaining only first-order terms, the angle rate differences are

$$\begin{aligned}\delta\dot{\lambda} = &-\left(\frac{3}{2a_0^{5/2}}\right)\delta a - \epsilon\left(\frac{21}{8a_0^{9/2}\eta_0^4}\right)\left[\eta_0\left(1-3\cos^2 i_0\right)+\left(1-5\cos^2 i_0\right)\right]\\ &\times\delta a + \epsilon\left(\frac{3}{4a_0^{7/2}\eta_0^5}\right)\left[\left[(9\eta_0+20)\cos^2 i_0-(3\eta_0+4)\right]\delta\eta\right.\\ &\left.+\eta_0\,(3\eta_0+5)\,\delta i\,\sin 2i_0\right] \qquad (8.8)\end{aligned}$$

$$\begin{aligned}\delta\dot{g} = &-\epsilon\left(\frac{21}{8a_0^{9/2}\eta_0^4}\right)\left(1-5\cos^2 i_0\right)\delta a\\ &+\epsilon\left(\frac{3}{4a_0^{7/2}\eta_0^5}\right)\left[(5\eta_0\sin 2i_0)\,\delta i-4\left(1-5\cos^2 i_0\right)\delta\eta\right] \qquad (8.9)\end{aligned}$$

$$\begin{aligned}\delta\dot{\hbar} = &-\epsilon\left(\frac{21}{4a_0^{9/2}\eta_0^4}\right)\cos i_0\delta a\\ &-\epsilon\left(\frac{3}{2a_0^{7/2}\eta_0^5}\right)(4\delta\eta\cos i_0+\eta_0\delta i\,\sin i_0) \qquad (8.10)\end{aligned}$$

Per the discussion above, instead of $\delta\dot{\lambda}$ we want to use $\left(\delta\dot{\lambda}+\delta\dot{\hbar}\cos i_0\right)$, which is given by

$$\begin{aligned}\left(\delta\dot{\lambda}+\delta\dot{\hbar}\cos i_0\right) = &-\left(\frac{3}{2a_0^{5/2}}\right)\delta a\\ &-\epsilon\left(\frac{3}{4a_0^{9/2}\eta_0^4}\right)(1+\eta_0)\left(1-3\cos^2 i_0\right)\delta a\\ &-\epsilon\left(\frac{3}{4a_0^{7/2}\eta_0^5}\right)(3\eta_0+4)\left[\left(1-3\cos^2 i_0\right)\delta\eta-(\eta_0\sin 2i_0)\,\delta i\right] \qquad (8.11)\end{aligned}$$

Note that the initial values of the angle differences $(\delta l, \delta g, \delta\hbar)$ have no effect on the drift; only the differences in the momenta $(\delta L, \delta G, \delta H)$ or $(\delta a, \delta\eta, \delta i)$ affect the drift. To prevent drift between the satellites we want $\delta\dot{\lambda}+\delta\dot{\hbar}\cos i_0 = \delta\dot{g} = \delta\dot{\hbar} = 0$. The drift can be controlled by thrusting but, depending on the desired formation, the amount of fuel required could be prohibitive. What we are investigating here is how to adjust the initial conditions, i.e., $(\delta a, \delta\eta, \delta i)$, to minimize the amount of fuel required to maintain the desired formation.

Equations (8.9), (8.10) and (8.11) are three equations with three unknowns, $(\delta a, \delta\eta, \delta i)$. The only solution is the trivial solution if the determinant of the coefficients is not equal to zero. This singular case will be ignored for the

moment. Except for the singular case, setting any of the differential angle rates, $(\delta\dot{\lambda}, \delta\dot{g}, \delta\dot{\hbar})$, establishes a constraint on the formation design.

The equations can be solved by inverting the matrix of coefficients, but a simpler approach is possible. Note that these equations are infinite series truncated at first-order, i.e., $\mathcal{O}(\epsilon)$. From Eq. (8.11) we see that $\delta a = \mathcal{O}(\epsilon)$. Therefore, we can neglect the δa terms in Eqs. (8.9) and (8.10). This simplifies the solutions and they are just as accurate as the solutions obtained from inverting the 3×3 matrix. The solutions to Eqs. (8.9), (8.10) and (8.11) are

$$\delta a = -\epsilon \left(\frac{1}{2a_0\eta_0^5}\right)(3\eta_0 + 4)\left[\left(1 - 3\cos^2 i_0\right)\delta\eta - (\eta_0 \sin 2i_0)\,\delta i\right] \tag{8.12}$$

$$\delta\eta = \frac{5\eta_0 \sin 2i_0}{4\left(1 - 5\cos^2 i_0\right)}\delta i \tag{8.13}$$

$$\delta\eta = -\frac{\eta_0 \tan i_0}{4}\delta i \tag{8.14}$$

Obviously, the only solution to Eqs. (8.13) and (8.14) is the trivial solution, $\delta\eta = \delta i = 0$. Either or both of these constraints may be incompatible with the desired mission. If only one or neither of these constraints is used, then Eq. (8.12) provides the δa that negates the along-track drift between the satellites. Since negating the along-track drift with this value of δa does not affect or constrain the choice of formations, this constraint should always be used. In terms of dimensional coordinates, it is

$$\delta a = 0.5 J_2 a_0 \left(\frac{R_e}{a_0}\right)^2 \left(\frac{3\eta_0 + 4}{\eta_0^5}\right) \times \left[\left(1 - 3\cos^2 i_0\right)\delta\eta - (\eta_0 \sin 2i_0)\,\delta i\right] \tag{8.15}$$

The effect of the constraints given by Eqs. (8.12), (8.13) and (8.14) on the formation design and the associated fuel to maintain the formation are now investigated.

8.1.1 Three constraints

As discussed above the three constraints are

$$\delta a = \delta i = \delta\eta = \delta e = 0 \tag{8.16}$$

This means the only freedom in the formation design is in the selection of the initial values of δl, δg, and $\delta\hbar$. The only formations possible with these three constraints are a leader–follower with some cross-track motion resulting from the differential right ascension, $\delta\hbar$, or $\delta\Omega$. These formations can be characterized as a dog wagging its tail. If the reference or chief orbit is eccentric, the along-track separation will be periodic with a period equal to the anomalistic

period. Different types of along-track motion occur depending on the selection of the initial values of δl and δg.

Consider two cases with the chief orbit having a small eccentricity and $(\delta l + \delta g) = K$, a constant. In the first case $\delta l = 0$, $\delta g = K$. This corresponds to two ellipses with different arguments of perigee and both objects are at perigee and apogee at the same time. The result is a constant angular separation of the two satellites and the in-plane separations at perigee and apogee are

$$d_p \approx a_0(1 - e_0)\ K, \quad d_a \approx a_0(1 + e_0)\ K. \tag{8.17}$$

In the second case select $\delta l = K$, $\delta g = 0$. In this case the ellipses coincide and the two satellites are in the same orbit, but just separated by a constant mean anomaly difference. Using $\delta \nu \approx \delta l(1 + 2e\cos l)$ the separations at perigee and apogee are

$$d_p \approx a_0(1 + e_0)\ K, \quad d_a \approx a_0(1 - e_0)\ K \tag{8.18}$$

This is exactly the opposite to case one, the maximum separation is at perigee and the minimum separation is at apogee. Since there is no drift, no fuel is required to negate the drift. However, if there is cross-track motion, the relative motion orbit will not be periodic. The in-plane and cross-track motions have different periods due to the rotation of perigee of the chief's orbit. The only way to negate this is by thrusting or to be at the critical inclination. There is another inclination [139] at which the difference between the in-plane and cross-track frequencies is minimized. Except for very small eccentricities, the fuel for controlling perigee is prohibitive. The Δv to negate perigee rotation for near circular orbits is (cf. the GVE in Section 2.5.4 and Ref. [144])

$$\Delta v \approx 0.75 J_2 \pi \sqrt{\frac{\mu}{a_0}} \left(\frac{R_e}{a_0}\right)^2 \left(1 - 5\cos^2 i_0\right) e_0 \text{ m/s/orbit} \tag{8.19}$$

For $a = 7500$ km, the annual Δv is

$$\Delta v \approx 65.6 \left(1 - 5\cos^2 i_0\right) e_0 \text{ km/s/yr} \tag{8.20}$$

Thus, unless $e_0 < 0.0001$ or $i_0 \approx 63.4°$ the fuel required to maintain perigee will be prohibitive.

Recall that $\eta^2 = (1 - e^2)$. Consequently, $\delta\eta = -e_0\delta e/\eta_0$. Therefore, for near-circular orbits, the primary effect on δa will be that due to the cross-track motion resulting from δi. Only for highly-elliptic orbits will the differential eccentricity have an effect on the semimajor axis adjustment.

8.1.2 Two constraints

As discussed above, the along-track drift negation constraint given by Eq. (8.12) should always be implemented because its use does not impact the formation design. Therefore, this is one of the two constraints. There are two options

for the second constraint: Negating the differential nodal precession or the differential perigee rotation. These constraints are given in Eqs. (8.14) and (8.13), respectively. The effect of the differential perigee rotation is a slow radial drift. There is no along-track drift due to the along-track drift constraint. What is happening here is a slow relative rotation of the two ellipses. For orbits with a small eccentricity, this effect is generally less than the differential nodal precession. However, for highly eccentric orbits, such as the NASA MMS mission, the differential perigee rotation effect can be larger than the differential nodal precession.

DIFFERENTIAL NODAL PRECESSION NEGATION

First, consider low near-circular orbits with the chief orbit semimajor axis $a = 7500$ km and vary the chief eccentricity and inclination. Note that for near-polar orbits, due to the $\tan i$ term in Eq. (8.14), if the cross-track motion is created with a δi, then $\delta\eta$ will have to be large, resulting in a large relative motion orbit; this is likely to be impractical. Conversely, the δi required to counter the effect of a prescribed $\delta\eta$ will be very small for near polar orbits.

Let the relative motion orbit have an average cross-track component of 1 km, consequently, $\delta i = 1/7500$ rad. Figure 8.1 shows the differential eccentricity required to negate the nodal precession as a function of eccentricity for various inclinations. For small eccentricities, the δe required is relatively large, likely too large for the desired formation. For example, for $e_0 = 0.01$ and $i_0 = 65°$ Eq. (8.14) gives, $\delta e = 0.0056$, resulting in a maximum radial difference of approximately 42 km. Note the case with $i = 95°$. For $e < 0.025$ the nodal precession cannot be negated. Figure 8.2 shows the differential semimajor axis to negate the along-track drift. As expected from the above discussion, it is essentially constant with increasing chief eccentricity, and is only a few meters. The relative motion orbits in this case of two constraints are called *J_2-invariant relative orbits* [32].

Now, consider highly eccentric orbits. Consider a critically inclined 12-hour orbit, $a_0 = 26{,}610$ km, and vary the eccentricity. The critical inclination was selected because control of perigee rotation is prohibitive for non-critical inclination highly eccentric orbits. The differential eccentricity required to negate the nodal precession is shown in Fig. 8.3 and the differential semimajor axis required to negate the along-track drift is shown in Fig. 8.4. Since the reference orbit is at the critical inclination, the in-plane and cross-track frequencies are equal and periodic relative motion orbits are possible. However, for each eccentricity and δi there is only one such relative motion orbit.

Using the constraint of Eq. (8.14), the approximate Δv per orbit required to negate the differential perigee rotation is

$$\Delta v = 0.75 J_2 \pi v_0 \left(\frac{R_e}{a_0}\right)^2 \left(\frac{e_0}{\eta_0^5}\right)\left(1 + 5\cos^2 i_0\right)\tan i_0 \delta i \text{ m/s/orbit} \quad (8.21)$$

or

$$\Delta v = 3 J_2 \pi v_0 \left(\frac{R_e}{a_0}\right)^2 \left(\frac{e_0}{\eta_0^5}\right)\left(1 + 5\cos^2 i_0\right)\delta\eta \text{ m/s/orbit} \quad (8.22)$$

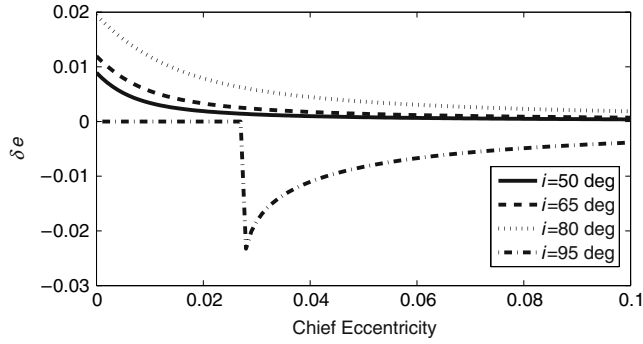

FIGURE 8.1 Differential eccentricity required to negate the differential nodal precession; small eccentricity.

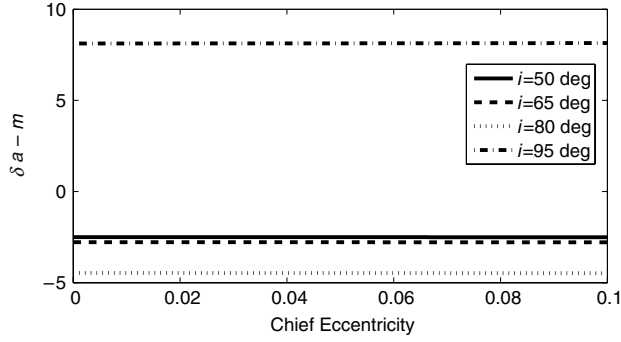

FIGURE 8.2 Differential semimajor axis required to negate the along-track drift; small eccentricity.

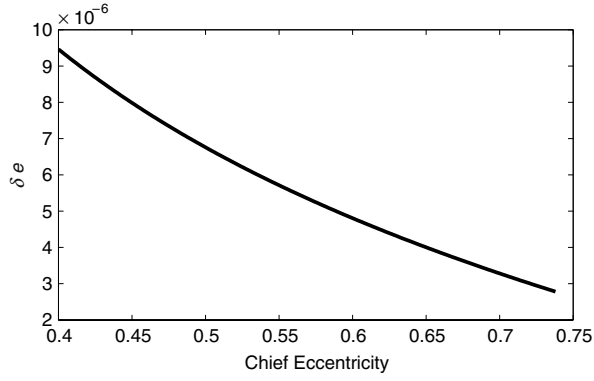

FIGURE 8.3 Differential eccentricity required to negate the differential nodal precession for a 12-hour orbit.

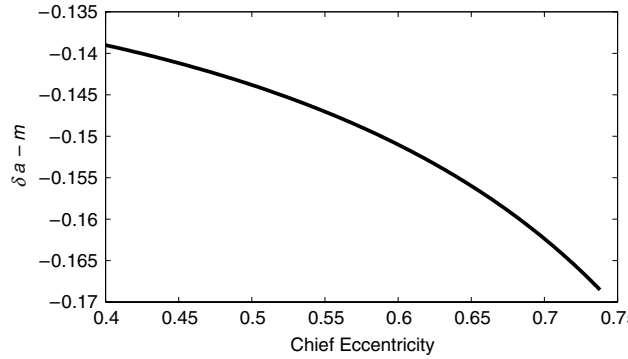

FIGURE 8.4 Differential semimajor axis required to negate the along-track drift for a 12-hour orbit.

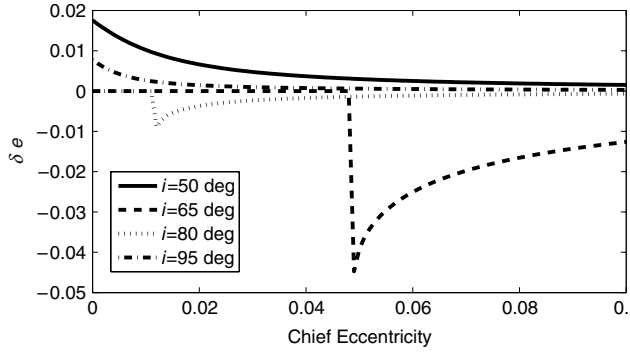

FIGURE 8.5 Differential eccentricity required to negate the differential perigee rotation.

where v_0 is the speed in a circular orbit with a radius equal to the semimajor axis, i.e., $r = a_0$. For a 7000 km near-circular chief orbit ($e_0 \approx 0$) with a 1 km cross-track motion caused by a differential inclination, the annual fuel requirement is $\Delta v = 45.1$ m/s/yr for $i_0 = 50°$. Even for moderate eccentricities, this is a small amount of fuel.

DIFFERENTIAL PERIGEE ROTATION NEGATION

To negate the differential perigee rotation, Eq. (8.13) is used to obtain $\delta\eta$. Figure 8.5 and 8.6 show the differential eccentricity and differential semimajor axis required to negate the differential perigee rotation and the along-track drift for the same low-Earth orbit example with $a_0 = 7500$ km. Figure 8.5 shows that when the chief eccentricity is small, it may not be possible to negate the differential perigee rotation. As with the differential nodal precession negation, this occurs when δe is negative and $|\delta e| > e_0$, which occurs for the cases $i_0 = 65°$ and $i_0 = 80°$. Figure 8.6 shows the same trend of an essentially constant δa of just a few meters, required to negate the along-track drift.

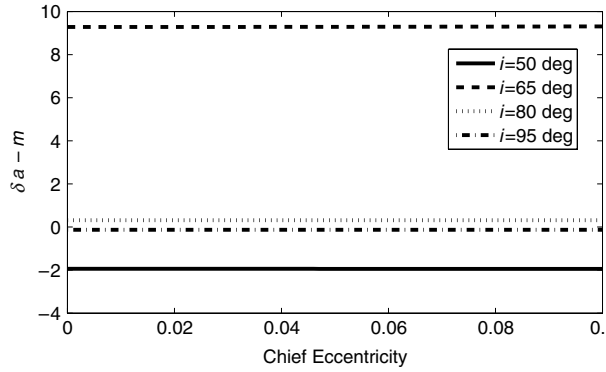

FIGURE 8.6 Differential semimajor axis required to negate the along-track drift.

Using the constraint Eq. (8.14), the approximate Δv per orbit required to negate the differential nodal rotation is

$$\Delta v = 1.2 J_2 \pi v_0 \left(\frac{R_e}{a_0}\right)^2 \left(\frac{\tan i_0}{\eta_0^4}\right) \left(1 + 5\cos^2 i_0\right) \delta\eta \text{ m/s/orbit} \quad (8.23)$$

or

$$\Delta v = 3 J_2 \pi v_0 \left(\frac{R_e}{a_0}\right)^2 \left(\frac{\sin^2 i_0}{\eta_0^3}\right) \frac{\left(1 + 5\cos^2 i_0\right)}{\left(1 - 5\cos^2 i_0\right)} \tan i_0 \, \delta i \text{ m/s/orbit} \quad (8.24)$$

For a 7000 km near circular chief orbit ($e_0 \approx 0$) with a 1 km cross-track motion caused by a differential inclination, the annual fuel requirement is $\Delta v = 83.4$ m/s/yr for $i_0 = 50°$. This supports the earlier statement that for near-circular orbits, the best approach is to negate the differential nodal precession, not the differential perigee rotation.

8.1.3 One constraint

As stated earlier, when there is only one constraint, it should be used for negating the along-track drift. The Δv per orbit for negating the differential nodal precession and differential perigee rotation are, respectively (cf. the GVE in Section 2.5.4),

$$\Delta v = 0.75 J_2 \pi v_0 \left(\frac{R_e}{a_0}\right)^2 \left(\frac{e_0}{\eta_0^6}\right) \left[5\eta_0 \delta i \sin 2i_0 + 4\delta\eta \left(5\cos^2 i_0 - 1\right)\right] \quad (8.25)$$

$$\Delta v = 3 J_2 \pi v_0 \left(\frac{R_e}{a_0}\right)^2 \left(\frac{\sin i_0}{\eta_0^4}\right) \left(\eta_0 \delta i \sin i_0 + 4\delta\eta \cos i_0\right) \quad (8.26)$$

8.1.4 Energy considerations

When there are no perturbations, the condition for periodic relative-motion orbits is that the semimajor axes be equal, i.e., $\delta a = 0$, which means that the energies of the two orbits are equal. This was referred to as the energy matching condition, discussed in Section 4.2. Now, let us revisit the energy matching condition when the J_2 perturbation exists. The mean energy of the orbit as a function of (a, i, η) is just the mean Hamiltonian given by Eqs. (3.19) and (3.20), with a proper substitution of the momenta L, G, H:

$$\bar{\mathcal{H}} = -\frac{1}{2a} - \frac{\epsilon}{4a^3\eta^3}\left(1 - 3\cos^2 i\right) \tag{8.27}$$

For a Keplerian motion, the energy is a function of only the semimajor axis, a. However, when J_2 is included, the energy depends on all three momenta elements (a, e, i). The mean energy difference $\delta\bar{\mathcal{H}}$ between a reference and a neighboring orbit is approximated by

$$\delta\bar{\mathcal{H}} = \bar{\mathcal{H}} - \bar{\mathcal{H}}_0 \approx \frac{\partial\bar{\mathcal{H}}_0}{\partial a}\delta a + \frac{\partial\bar{\mathcal{H}}_0}{\partial \eta}\delta\eta + \frac{\partial\bar{\mathcal{H}}_0}{\partial i}\delta i \tag{8.28}$$

where the subscript 0 denotes the reference orbit. Substituting for the partial derivatives and keeping in mind that $\delta a = \mathcal{O}(\epsilon)$ the energy difference becomes

$$\delta\bar{\mathcal{H}} = \frac{1}{2a_0^2}\delta a + \epsilon\frac{3}{4a_0^3\eta_0^4}\left[\left(1 - 3\cos^2 i_0\right)\delta\eta - (\eta_0 \sin 2i_0)\,\delta i\right] \tag{8.29}$$

Substituting Eq. (8.12) for δa gives

$$\delta\bar{\mathcal{H}} = -\frac{\epsilon}{a_0^3\eta_0^5}\left[\left(1 - 3\cos^2 i_0\right)\delta\eta - (\eta_0 \sin 2i_0)\,\delta i\right] \tag{8.30}$$

This means that for $\delta\bar{\mathcal{H}} = 0$, one has $\left(1 - 3\cos^2 i_0\right)\delta\eta = (\eta_0 \sin 2i_0)\,\delta i$. However, this condition does not negate either the differential nodal precession or differential perigee rotation unless $\delta\eta = \delta i = 0$. Therefore, equal energy orbits result in no along-track drift, but not differential nodal precession or differential perigee rotation. It is important to note that the condition of no along-track drift does not result in equal energy orbits except for specific singular cases such as $\delta i = 0$ and $\cos i_0 = 1/\sqrt{3}$.

Now, consider the energy difference for negation of the differential nodal precession. Substituting Eq. (8.14) into the energy difference equation, Eq. (8.30), gives

$$\delta\bar{\mathcal{H}} = \epsilon\left(\frac{\tan i_0}{4a_0\eta_0^5}\right)\left(1 + 5\cos^2 i_0\right)\delta i \tag{8.31}$$

Thus, $\delta\bar{\mathcal{H}} = 0$ only if $\delta i = \delta\eta = \delta a = 0$. A similar result is obtained for negating the differential perigee rotation.

8.1.5 Numerical results

THREE CONSTRAINTS

The following example is used to demonstrate the three-constraint case. Table 8.1 gives the mean orbital elements of the chief. The deputy trails the chief by a nominal distance of 1 km with a nominal cross-track motion of 1 km. The differential orbital elements are $\delta a = \delta\eta = \delta i = \delta l = 0$ and $\delta g = \delta\hbar = -1/a_0 = -0.0001429$ radians. With these differential elements there should be no drift in any direction. However, the mean-to-osculating transformation is not exact; it is correct only to first order, so some minor drift will occur. In addition, the in-plane and out-of-plane frequencies are different; therefore, the relative motion orbit will not be periodic.

With the chosen orbital element values, the perigee rotation period is approximately 70 days. Hence, it will take 17.5 days to obtain a 90-degree phase shift between the out-of-plane and in-plane motions. The purpose of the simulations is to (a) illustrate the effectiveness of the three constraints $\delta a = \delta\eta = \delta i = 0$ in maintaining a formation in close proximity, i.e., no drift, and (b) to demonstrate the negative effect of neglecting the effect of J_2 in developing the initial conditions. This is implemented by assuming that the mean elements are osculating elements. The truth orbits for both the chief and deputy were determined by numerically integrating the equations of motion with $J_2 - J_5$. The elements given in Table 8.1 are mean elements for the chief satellite. The deputy mean elements are obtained by adding the differential elements to the chief elements. Both are then transformed to osculating elements and the equations of motion are numerically integrated.

Figure 8.7 shows the 3D relative motion orbit for approximately three days. With the mean element initial conditions, the relative motion trajectory is nearly periodic. The beginning of the effect of the absolute perigee rotation is evident with the thickness of the line. Obviously, neglecting J_2 in determining the initial conditions creates a problem: The relative motion trajectory deteriorates quickly. The drift that occurs in the along-track direction, resulting from neglecting J_2 in determining the initial conditions, is also evident in Fig. 8.8. With the mean element initial conditions, there is essentially no drift. The minor drift results from the neglected higher-order terms, which are $\mathcal{O}(J_2^2)$. When assuming that the initial mean elements are osculating elements, the along-track drift occurs at a rate of about 200 meters per day; this drift would have to be negated with control. Furthermore, if the J_2 effect were neglected, the control system would return the system to the same desired differential elements and the drift would continue.

TWO CONSTRAINTS

The initial values of the chief orbital elements for the two-constraints simulations are given in Table 8.2. The maximum cross-track motion is to be approximately 1 km and created by an inclination difference, which gives $\delta i = 1/a_0$. We want to negate the cross-track drift, so the second constraint, Eq. (8.14), gives $\delta e = 0.001366$. The corresponding differential semimajor axis required

Table 8.1 Chief satellite orbital elements; three-constraints case

Desired mean orbit elements	Value	Units
a	7100	km
e	0.05	
i	50	deg
$\hbar$	0.0	deg
g	30.0	deg
l	0.0	deg

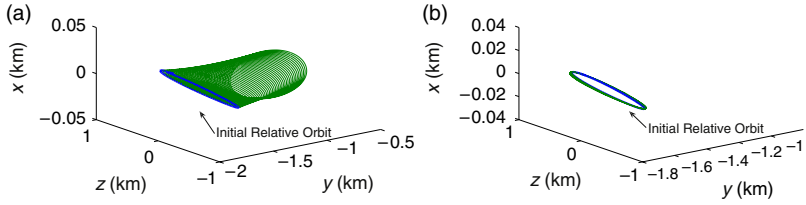

FIGURE 8.7 (a) Initial relative orbit setup in osculating elements. (b) Initial relative orbit setup in mean elements.

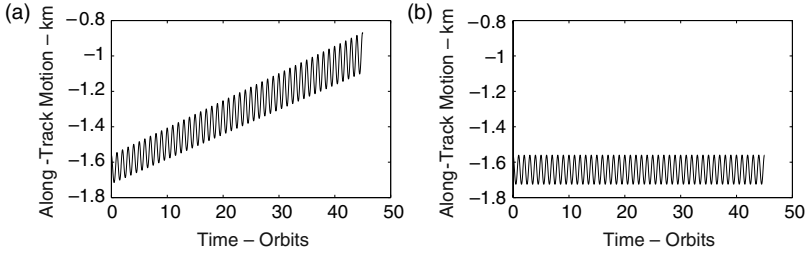

FIGURE 8.8 (a) Along-track relative motion for osculating element setup. (b) Along-track relative motion for mean element setup.

to negate the along-track drift is $\delta a = -2.5089$ m. The other differential elements are $\delta g = \delta\hbar = 0, \delta l = 2\delta e$. This choice of δl centers the formation on the chief. The along-track dimension of the formation is approximately 20.5 km, 10 times the cross-track.

Figure 8.9 shows the relative motion orbit for three days with and without the along-track constraint. The value of the constraint in maintaining the formation is evident. Figure 8.10 shows the along-track motion without and with the along-track constraint. The along-track drift, d_{drift}, per orbit is $d_{\text{drift}} = 3\pi\delta a$. Thus, not using the along-track constraint of $\delta a = -2.5089$ m should result in

Table 8.2 Chief satellite orbital elements; two-constraints case

Desired mean orbit elements	Value	Units
a	7500	km
e	0.1	
i	50	deg
$\hbar$	0.0	deg
g	0.0	deg
l	0.0	deg

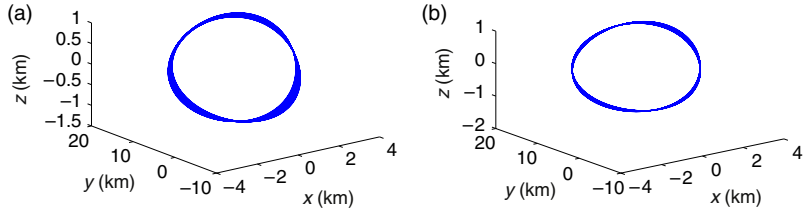

FIGURE 8.9 (a) Relative motion orbit without along-track negation. (b) Relative motion orbit with along-track negation.

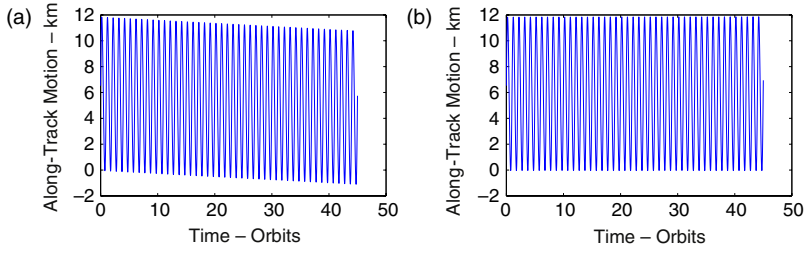

FIGURE 8.10 (a) Along-track time history without along-track constraint. (b) Along-track time history with along-track constraint.

a drift of approximately 316 m/day. The along-track drift in Fig. 8.10 is about 1 km over three days, about the expected value. The right ascension time history is shown in Fig. 8.11 and illustrates the effectiveness of the J_2 invariant orbit in suppressing the cross-track growth.

The next simulation uses the same chief elements as the previous one, but the relative motion orbit is selected to be similar to the projected circular orbit (see Eq. (5.36)) of radius 1 km with the cross-track motion created by an ascending node difference. The differential elements are $\delta e = 1/2a_0$, $\delta\hbar = 1/(a_0 \sin i_0)$, and $\delta l = \delta g = 0$. The constraints for negating the differential nodal precession and the along-track drift give $\delta a = -0.425$ m and $\delta i = 0.00013°$. Note that

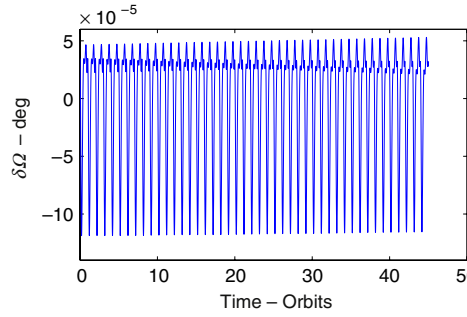

FIGURE 8.11 Differential right ascension time history.

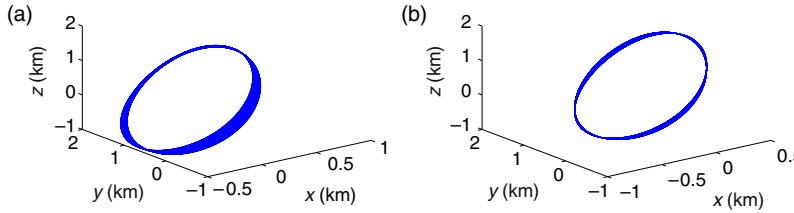

FIGURE 8.12 (a) Relative motion orbit without along-track negation. (b) Relative motion orbit with along-track negation.

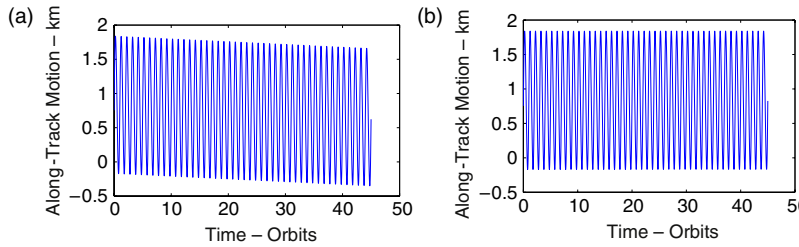

FIGURE 8.13 (a) Along-track time history without along-track constraint. (b) Along-track time history with along-track constraint.

these values are much less than the previous case. This demonstrates that δi has a much larger effect on the differential element constraints than δe. Figure 8.12 shows the 3D relative motion orbit without and with the along-track constraint. The drift is evident when the along-track constraint of $\delta a = -0.425$ m is not used. Figure 8.13 shows the along-track motion without and with the along-track constraint. The drift is much less in this case because the cross-track motion is caused by a differential right ascension, not a differential inclination. Figure 8.14 shows again the effectiveness in suppressing any cross-track growth.

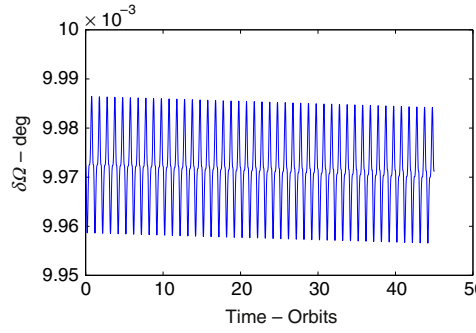

FIGURE 8.14 Differential right ascension time history.

ONE CONSTRAINT

The one-constraint case uses only the constraint on δa to negate the along-track drift. The effectiveness of using this constraint was demonstrated previously, so no separate results are presented here. Figure 8.14 shows that when the cross-track motion is created by a node difference, not an inclination difference, then the cross-track constraint is not nearly as important.

8.2 A NONLINEAR THEORY BASED ON ORBITAL ELEMENTS

The CW equations assume that the Earth is spherically symmetric, the reference or chief orbit is circular, and that the ratio of the formation size is small compared to the chief radius, so that the differential gravity terms can be linearized in the local coordinates. Each of these assumptions causes errors in the solution. In Section 8.3 the effects of these modeling errors in the various theories, including the one developed in this section, are evaluated. This evaluation shows that the effect of not modeling J_2 effects and assuming a circular chief orbit generally dominate the errors for formation sizes smaller than 20–40 km. Therefore, except for very large formations, for a nonlinear theory to be useful for formation design and analysis it needs to also include the J_2 and chief orbit eccentricity effects. This results in a formidable problem.

The first attempt at incorporating nonlinear effects was performed by London [145]. He assumed a circular reference orbit and a spherical Earth, and expanded the differential gravity terms into a power series, retaining terms through second order. He then performed a perturbation analysis with the first-order solution being the CW equations to obtain an approximate solution through second order. The problem with this approach is that in the along-track solution the first-order terms have t terms and the second-order terms contain t^2 terms. For the solution to be uniformly valid,

$$\lim_{t\to\infty}\left(\frac{x_{n+1}}{x_n}\right) = \mathcal{O}(1) \tag{8.32}$$

where x_n is the nth-order solution. For London's solution

$$\lim_{t\to\infty}\left(\frac{x_{n+1}}{x_n}\right) = \epsilon t \tag{8.33}$$

where ϵ is a small parameter indicative of the ratio of the relative separation to the orbit radius. Thus, the solution is not uniformly valid; it is only valid for a short period of time. The perturbation approach does, however, improve the solution. Mitchell and Richardson [146] took the same approach to obtain the initial conditions for periodic solutions. Since the solution is periodic, it does not suffer from the uniform validity problem. However, it is only valid for circular reference orbits and does not include any J_2 effects. Vaddi *et al.* [147] expand the work of Mitchell and Richardson to include first-order eccentricity effects. Since they are also obtaining periodic solutions, their solution does not suffer from the uniform validity problem. The problem with the along-track secular terms is a result of the physics, not the perturbation approach. Bond [104] showed that the term leading to the secular term is actually $\sin(\Delta n t)/\Delta n$ where Δn is the difference in the mean motions of the chief and deputy. Expansion of this term gives the secular term at first-order and the higher-order terms in t at higher orders. Karlgaard and Lutze [148] take a different approach using spherical coordinates and multiple time scales to obtain a perturbation solution to second-order. Their solution is uniformly valid through second order. However, it is expected that the third-order solution would have higher-order terms in t, but the analysis has not been obtained to prove this. The reasoning is that the use of spherical coordinates results in the higher-order t terms not appearing before the third perturbation solution. The unit sphere approach of Section 7.1 is not a perturbation solution about the non-spherical Earth and does not suffer from these problems.

With the need to include gravitational effects and eccentric chief orbits, and the demonstrated evidence that differential orbital elements [149] result in the most accurate linear relative motion solution, it is advantageous to develop a perturbation solution in mean elements. In addition to the accuracy improvement with mean elements, the angles do not appear in the Hamiltonian, so there should be no $t^n, n > 1$ terms in the solution. Hence, the solution will be uniformly valid. The second-order state transition approach for propagating perturbed relative motion developed by Sengupta *et al.* [2], introduced in Section 7.7, uses an orbital elements approach but includes only the J_2 terms. The theory developed in this section includes $\mathcal{O}(J_2^2)$ terms.

We start with the averaged Hamiltonian, expanded to the second order, given by Eqs. (3.19), (3.20), and (3.23). The rates for the mean argument of latitude, argument of perigee and right ascension are given below. Since the formation is defined by differences in (a, e, i) or (L, e, i) it is preferable to have the angle rates as a function of (L, e, i) instead of (L, G, H). The angle rates as

a function of (L, e, i) are:[1]

$$\begin{aligned}
\dot{\lambda} &= \frac{\partial \bar{\mathcal{H}}}{\partial L} + \frac{\partial \bar{\mathcal{H}}}{\partial G} \\
\dot{\lambda} &= \frac{1}{L^3} + \epsilon \left(\frac{3}{4L^3\eta^4}\right)\left[(1+\eta) - (5+3\eta)\cos^2 i\right) + 0.5\epsilon^2 \left(\frac{3}{64L^{11}\eta^8}\right) \\
&\quad \times \left[\left(-35 + 9\eta + 41\eta^2 + 25\eta^3\right) + \left(90 - 162\eta - 222\eta^2 - 90\eta^3\right)\cos^2 i \right. \\
&\quad \left. + \left(385 + 465\eta + 189\eta^2 + 25\eta^3\right)\cos^4 i\right]
\end{aligned} \tag{8.34}$$

$$\begin{aligned}
\dot{g} &= \dot{\omega} = \frac{\partial \bar{\mathcal{H}}}{\partial G} \\
\dot{\omega} &= \epsilon \left(\frac{3}{4L^7\eta^4}\right)\left(1 - 5\cos^2 i\right) - 0.5\epsilon^2 \left(\frac{15}{320L^{11}\eta^8}\right) \\
&\quad \times \left[\left(35 - 24\eta - 25\eta^2\right) + \left(-90 + 192\eta + 126\eta^2\right)\cos^2 i \right. \\
&\quad \left. - \left(385 + 360\eta + 45\eta^2\right)\cos^4 i\right]
\end{aligned} \tag{8.35}$$

$$\begin{aligned}
\dot{\hbar} &= \dot{\Omega} = \frac{\partial \bar{\mathcal{H}}}{\partial H} \\
\dot{\Omega} &= \epsilon \left(\frac{3}{2L^7\eta^4}\right)\cos i - 0.5\epsilon^2 \left(\frac{3}{16L^{11}\eta^8}\right) \\
&\quad \left[\left(5 - 12\eta - 9\eta^2\right)\cos i + \left(35 + 36\eta + 5\eta^2\right)\cos^2 i\right]
\end{aligned} \tag{8.36}$$

The differential angle rates between two satellites in a formation are given below where the subscript "0" is used to represent the elements of the chief satellite. Since this is a nonlinear theory the Taylor series expansion is carried to second order, in contrast to the first-order expansion in the linear theories.

$$\begin{aligned}
\delta\dot{\lambda} &= \frac{\partial \dot{\lambda}}{\partial L}\delta L + \frac{\partial \dot{\lambda}}{\partial \eta}\delta\eta + \frac{\partial \dot{\lambda}}{\partial i}\delta i + \frac{1}{2}\frac{\partial^2 \dot{\lambda}}{\partial L^2}\delta L^2 + \frac{1}{2}\frac{\partial^2 \dot{\lambda}}{\partial \eta^2}\delta\eta^2 \\
&\quad + \frac{1}{2}\frac{\partial^2 \dot{\lambda}}{\partial i^2}\delta i^2 + \frac{\partial^2 \dot{\lambda}}{\partial L \partial \eta}\delta L\delta i + \frac{\partial^2 \dot{\lambda}}{\partial L \partial i}\delta L\delta i + \frac{\partial^2 \dot{\lambda}}{\partial L \partial \eta}\delta\eta\delta i
\end{aligned} \tag{8.37}$$

$$\begin{aligned}
\delta\dot{\omega} &= \frac{\partial \dot{\omega}}{\partial L}\delta L + \frac{\partial \dot{\omega}}{\partial \eta}\delta\eta + \frac{\partial \dot{\omega}}{\partial i}\delta i + \frac{1}{2}\frac{\partial^2 \dot{\omega}}{\partial L^2}\delta L^2 + \frac{1}{2}\frac{\partial^2 \dot{\omega}}{\partial \eta^2}\delta\eta^2 \\
&\quad + \frac{1}{2}\frac{\partial^2 \dot{\omega}}{\partial i^2}\delta i^2 + \frac{\partial^2 \dot{\omega}}{\partial L \partial \eta}\delta L\delta i + \frac{\partial^2 \dot{\omega}}{\partial L \partial i}\delta L\delta i + \frac{\partial^2 \dot{\omega}}{\partial L \partial \eta}\delta\eta\delta i
\end{aligned} \tag{8.38}$$

$$\begin{aligned}
\delta\dot{\Omega} &= \frac{\partial \dot{\Omega}}{\partial L}\delta L + \frac{\partial \dot{\Omega}}{\partial \eta}\delta\eta + \frac{\partial \dot{\Omega}}{\partial i}\delta i + \frac{1}{2}\frac{\partial^2 \dot{\Omega}}{\partial L^2}\delta L^2 + \frac{1}{2}\frac{\partial^2 \dot{\Omega}}{\partial \eta^2}\delta\eta^2 \\
&\quad + \frac{1}{2}\frac{\partial^2 \dot{\Omega}}{\partial i^2}\delta i^2 + \frac{\partial^2 \dot{\Omega}}{\partial L \partial \eta}\delta L\delta i + \frac{\partial^2 \dot{\Omega}}{\partial L \partial i}\delta L\delta i + \frac{\partial^2 \dot{\Omega}}{\partial L \partial \eta}\delta\eta\delta i
\end{aligned} \tag{8.39}$$

[1] We actually use η instead of e, where $\eta^2 = (1 - e^2)$.

Now obtain the partial derivatives of the angle rates given in Eqs. (8.34)–(8.36) and let

$$\begin{aligned}
&\frac{\partial \dot{\lambda}}{\partial L} = a_{10} + \epsilon a_{11} + 0.5\epsilon^2 a_{12}, \ \frac{\partial \dot{\lambda}}{\partial \eta} = \epsilon a_{21} + 0.5\epsilon^2 a_{22} \\
&\frac{\partial \dot{\lambda}}{\partial i} = \epsilon a_{31} + 0.5\epsilon^2 a_{32}, \ \frac{\partial^2 \dot{\lambda}}{\partial L^2} = a_{40} + \epsilon a_{41} + 0.5\epsilon^2 a_{42} \\
&\frac{\partial^2 \dot{\lambda}}{\partial \eta^2} = \epsilon a_{51} + 0.5\epsilon^2 a_{52}, \ \frac{\partial^2 \dot{\lambda}}{\partial i^2} = \epsilon a_{61} + 0.5\epsilon^2 a_{62} \\
&\frac{\partial^2 \dot{\lambda}}{\partial L \partial \eta} = \epsilon a_{71} + 0.5\epsilon^2 a_{72}, \ \frac{\partial^2 \dot{\lambda}}{\partial L \partial i} = \epsilon a_{81} + 0.5\epsilon^2 a_{82} \\
&\frac{\partial^2 \dot{\lambda}}{\partial \eta \partial i} = \epsilon a_{91} + 0.5\epsilon^2 a_{92}
\end{aligned} \tag{8.40}$$

$$\begin{aligned}
&\frac{\partial \dot{\omega}}{\partial L} = \epsilon b_{11} + 0.5\epsilon^2 b_{12}, \ \frac{\partial \dot{\omega}}{\partial \eta} = \epsilon b_{21} + 0.5\epsilon^2 b_{22} \\
&\frac{\partial \dot{\omega}}{\partial i} = \epsilon b_{31} + 0.5\epsilon^2 b_{32}, \ \frac{\partial^2 \dot{\omega}}{\partial L^2} = \epsilon b_{41} + 0.5\epsilon^2 b_{42} \\
&\frac{\partial^2 \dot{\omega}}{\partial \eta^2} = \epsilon b_{51} + 0.5\epsilon^2 b_{52}, \ \frac{\partial^2 \dot{\omega}}{\partial i^2} = \epsilon b_{61} + 0.5\epsilon^2 b_{62} \\
&\frac{\partial^2 \dot{\omega}}{\partial L \partial \eta} = \epsilon b_{71} + 0.5\epsilon^2 b_{72}, \ \frac{\partial^2 \omega}{\partial L \partial i} = \epsilon b_{81} + 0.5\epsilon^2 b_{82} \\
&\frac{\partial^2 \dot{\omega}}{\partial \eta \partial i} = \epsilon b_{91} + 0.5\epsilon^2 b_{92}
\end{aligned} \tag{8.41}$$

$$\begin{aligned}
&\frac{\partial \dot{\Omega}}{\partial L} = \epsilon c_{11} + 0.5\epsilon^2 c_{12}, \ \frac{\partial \dot{\Omega}}{\partial \eta} = \epsilon c_{21} + 0.5\epsilon^2 c_{22} \\
&\frac{\partial \dot{\Omega}}{\partial i} = \epsilon c_{31} + 0.5\epsilon^2 c_{32}, \ \frac{\partial^2 \dot{\Omega}}{\partial L^2} = \epsilon c_{41} + 0.5\epsilon^2 c_{42} \\
&\frac{\partial^2 \dot{\Omega}}{\partial \eta^2} = \epsilon c_{51} + 0.5\epsilon^2 c_{52}, \ \frac{\partial^2 \dot{\Omega}}{\partial i^2} = \epsilon c_{61} + 0.5\epsilon^2 c_{62} \\
&\frac{\partial^2 \dot{\Omega}}{\partial L \partial \eta} = \epsilon c_{71} + 0.5\epsilon^2 c_{72}, \ \frac{\partial^2 \Omega}{\partial L \partial i} = \epsilon c_{81} + 0.5\epsilon^2 a_{82} \\
&\frac{\partial^2 \dot{\Omega}}{\partial \eta \partial i} = \epsilon c_{91} + 0.5\epsilon^2 c_{92}
\end{aligned} \tag{8.42}$$

The a_{ij}, b_{ij}, c_{ij} coefficients are given in Appendix H.

Now consider the size of the relative motion orbit. If $\delta i = \mathcal{O}(\epsilon)$ and/or $\delta e = \mathcal{O}(\epsilon)$, then the size of the relative motion orbit can be several hundred kilometers. Therefore, assume $\delta i = \mathcal{O}(\epsilon)$ and $\delta e = \mathcal{O}(\epsilon)$. If they are smaller,

that is no problem. Since $\eta\delta\eta = -e\delta e$, the order of magnitude of $\delta\eta$ depends on the value of e and δe. We will assume that $\delta\eta = \mathcal{O}(\epsilon)$. Again, if it is smaller there is no problem. With these assumptions, and based on the J_2 invariant orbits research and Eq. (8.37), we see that $\delta L = \mathcal{O}(\epsilon^2)$. Therefore, set

$$\begin{aligned}\delta L &= \epsilon^2\delta L_2 + \epsilon^3\delta L_3\\ \delta\eta &= \epsilon\delta\eta_1 + \epsilon^2\delta\eta_2\\ \delta i &= \epsilon\delta i_1 + \epsilon^2\delta i_2\end{aligned} \tag{8.43}$$

Now substitute Eqs. (8.42)– (8.43) into Eqs. (8.34)–(8.36) and equate terms of like powers of ϵ.

$$\begin{aligned}\delta\dot{\lambda} = &\left(a_{10}\delta L_2 + a_{21}\delta\eta_1 + a_{31}\delta i_1\right)\epsilon^2 + \left(a_{11}\delta L_2 + a_{10}\delta L_3 + a_{21}\delta\eta_2\right.\\ &+ a_{31}\delta i_2 + 0.5a_{22}\delta\eta_1 + 0.5a_{32}\delta i_1 + 0.5a_{51}\delta\eta_1^2\\ &\left.+ 0.5a_{61}\delta i_1^2 + a_{91}\delta\eta_1\delta i_1\right)\end{aligned} \tag{8.44}$$

$$\begin{aligned}\delta\dot{\omega} = &\left(b_{21}\delta\eta_1 + b_{31}\delta i_1\right)\epsilon^2 + \left(b_{11}\delta L_2 + b_{21}\delta\eta_2 + b_{31}\delta i_2\right.\\ &\left.+ 0.5b_{22}\delta\eta_1 + 0.5b_{32}\delta i_1 + 0.5b_{51}\delta\eta_1^2 + 0.5b_{61}\delta i_1^2 + b_{91}\delta\eta_1\delta i_1\right)\end{aligned} \tag{8.45}$$

$$\begin{aligned}\delta\dot{\Omega} = &\left(c_{21}\delta\eta_1 + c_{31}\delta i_1\right)\epsilon^2 + \left(c_{11}\delta L_2 + c_{21}\delta\eta_2 + c_{31}\delta i_1\right.\\ &\left.+ 0.5c_{22}\delta\eta_1 + 0.5c_{32}\delta i_1 + 0.5c_{51}\delta\eta_1^2 + 0.5c_{61}\delta i_1^2 + c_{91}\delta\eta_1\delta i_1\right)\end{aligned} \tag{8.46}$$

Setting any of these three equations equal to zero provides a constraint on the relative motion. The impact of each of the $\mathcal{O}(\epsilon^2)$, linear theory, constraints on the relative motion and design of satellite formations was investigated in Section 8.1. The effect of one, two and three constraints were investigated with the $\delta\dot{\lambda} = 0$ constraint being replaced by $\delta\dot{\lambda} + \delta\dot{\Omega}\cos i = 0$, which is the no along-track drift condition. Just as with the linear theory, the only solution with all three constraints is the trivial solution, $\delta L = \delta\eta = \delta i = 0$. However, the no along-track drift constraint is a linear theory constraint, not a nonlinear theory constraint. The linear no along-track drift constraint from Eqs. (8.44)–(8.46) is

$$\delta L_2 = -\epsilon\frac{(3\eta_0 + 4)}{4L_0^3\eta_0^5}\left[\left(1 - 3\cos^2 i_0\right)\delta\eta - \left(\eta_0 \sin 2i_0\right)\delta i\right] \tag{8.47}$$

or

$$\begin{aligned}\delta a = &\, 0.5J_2 a_0\left(\frac{R_e}{a_0}\right)^2\left(\frac{3\eta_0 + 4}{2\eta_0^5}\right)\\ &\times\left[\left(1 - 3\cos^2 i_0\right)\delta\eta - \left(\eta_0 \sin 2i_0\right)\delta i\right]\end{aligned} \tag{8.48}$$

The second-order correction for the semimajor axis for the linear no along-track drift constraint is

$$\begin{aligned} a_{10}\delta L_3 = &-(a_{11}+c_{11}\cos i)\,\delta L_2 \\ &-(a_{21}+c_{21}\cos i)\,\delta\eta_2-(a_{31}+c_{31}\cos i)\,\delta i_2 \\ &-0.5\,(a_{22}+c_{22}\cos i)\,\delta\eta_1-0.5\,(a_{32}+c_{32}\cos i)\,\delta i_1\delta\eta_1^2 \\ &-0.5\,(a_{31}+c_{31}\cos i)-0.5\,(a_{61}+c_{61}\cos i)\,\delta i_1^2 \\ &-(a_{91}+c_{91}\cos i)\,\delta\eta_1\delta i_1 \end{aligned} \tag{8.49}$$

Again, it is important to point out that this is not a nonlinear constraint, it is the linear constraint that includes the higher-order terms in the expansion. The nonlinear no along-track drift condition is an open question at this time.

The constraint for no out-of-plane drift is $\delta\dot{\Omega}=0$. The first-order constraint from Eq. (8.46) is

$$\delta\eta_1 = -(0.25\eta_0\tan i_0)\delta i_1 \tag{8.50}$$

which is identical to Eq. (8.14) in Section 8.1. As shown in Section 8.1, if the out-of-plane motion is created by a differential inclination and the chief orbit is near-circular or near-polar, then the required eccentricity will result in a large formation, and is likely not feasible. Substituting Eq. (8.50) into Eq. (8.46) and setting it equal to zero gives the solution for $\delta\eta_2$ and δi_2:

$$\begin{aligned} c_{21}\delta\eta_2+c_{31}\delta i_2 = &-c_{11}\delta L_2-0.5c_{22}\delta\eta_1-0.5c_{32}\delta i_1-0.5c_{51}\delta\eta_1^2 \\ &-0.5c_{61}\delta i_1^2-c_{91}\delta\eta_1\delta i_1 \end{aligned} \tag{8.51}$$

All of the potential cases are beyond the scope of discussion, but for the use of this theory some discussion is in order. Consider first the case of one constraint, the no along-track drift constraint, and that δi and $\delta\eta$ are defined by the desired formation. Also assume that the no along-track drift constraint is the linear theory constraint $\delta\dot{\lambda}+\delta\dot{\Omega}\cos i=0$. Then set $\delta\eta_1=\delta\eta, \delta i_1=\delta i$ and $\delta\eta_2=\delta i_2=0$ and compute δL_2 and δL_3 using Eqs. (8.47) and (8.49). These provide the mean momenta and then with the mean differential angles $(\delta l, \delta\omega, \delta\Omega)$ defined by the formation obtain the mean deputy elements and transform to osculating elements to obtain the initial conditions. Now consider the two constraint case and assume the second constraint is negation of the out-of-plane drift, $\delta\dot{\Omega}=0$. Also assume that the formation defines δe. Then compute $\delta\eta$ from

$$\delta\eta = \sqrt{1-(e_0+\delta e)^2}-\sqrt{1-e_0^2} \tag{8.52}$$

Set $\delta\eta_1=\delta\eta$ and $\delta\eta_2=0$. Then compute δi_1 using Eq. (8.50), δL_2 using Eq. (8.47), δi_2 using Eq. (8.51), and δL_3 using Eq. (8.49). Then,

$$\delta L = \epsilon^2\delta L_2+\epsilon^3\delta L_3,\ \ \delta i = \epsilon\delta i_1+\epsilon^2\delta i_2 \tag{8.53}$$

With the angles defined by the formation, the mean elements are now defined. Transform to osculating elements to obtain the osculating elements and corresponding position and velocity.

To investigate the effect of adding the nonlinear effects to the model, consider the following example.

Example 8.1. *Choose a projected circular orbit (PCO) with the out-of-plane motion created by a differential inclination. The initial mean elements of the chief are:*

$$a_0 = 8000 \text{ km}, \quad e_0 = 0.01, \quad i_0 = 50^\circ \tag{8.54}$$
$$M_0 = \omega_0 = \Omega_0 = 0$$

Using Ref. [123], the initial differential mean elements of the deputy are:

$$\delta q_1 = 0, \quad \delta q_2 = -\frac{\rho}{2a_0} \tag{8.55}$$
$$\delta i = \frac{\rho}{a_0}, \quad \delta\Omega = 0, \quad \delta\lambda = 0$$

To evaluate the accuracy of the no along-track drift computation as a function of the formation size, the PCO radius is varied from 800 m to 160 km. The differential semimajor axis to negate the along-track drift is computed in four ways: (i) using the first-order no along-track drift condition, Eq. (8.48); (ii) using the second-order correction, Eqs. (8.47) and (8.49) without the J_2^2 term in the Hamiltonian; (iii) using the second-order correction, Eqs. (8.47) and (8.49) with the J_2^2 term in the Hamiltonian; and (iv) a numerical method. The numerical method is performed by numerically integrating the equations of motion of the chief and deputy for 10 orbits, differencing them to obtain the along-track motion, averaging it and then iterating to find the differential semimajor axis that negates the along-track secular drift in the averaged along-track motion. More details are given in Ref. [150].

Table 8.3 shows the results. The along-track drift per orbit is given by $d = 3\pi\delta a$. With the numerical δa as the value that results in no drift, the drift that occurs with each of the approximations can be obtained by using for δa in the drift equation the difference between the numerical δa and the δa for the approximation. For an 8 km PCO radius the error in δa using the first-order or linear theory is only 3.6 cm. Including the second-order effects, but without including the J_2^2 terms in the Hamiltonian only reduces the error to 2 cm, whereas including the terms in the Hamiltonian reduces the error to less than 0.1 mm. For the 160 km PCO, the error in δa from the nonlinear theory when including the J_2^2 terms in the Hamiltonian is only 1.5 cm, but the linear along-track drift condition results in an error of 2.6 m, which leads to a drift of 25 m/orbit. It should be noted that using the CW equations results in a δa error equal to that in the last column because $\delta a = 0$ for no drift when using the CW equations. Keeping in mind that these results were computed for the more stressing condition where the out-of-plane motion is caused completely

Table 8.3 δa (m) For no along-track drift

ρ (km)	First-order	Second-order without J_2^2	Second-order with J_2^2	Numerical
0.80	−0.1879	−1.8968	−1.8948	−1.8948
1.60	−3.7958	−3.7934	−3.7895	−3.7895
4.00	− 9.4895	−9.4828	−9.4730	−9.4730
8.00	− 18.9790	−18.9632	−18.9435	−18.9435
16.00	− 37.9580	−37.9167	−37.8775	−37.8774
40.00	− 94.8950	−94.7189	−94.6218	−94.6199
80.00	− 189.7901	−189.1948	−189.0039	−188.9892
160.00	− 379.5801	−377.4179	−377.0487	−376.9339

by a differential inclination, one can conclude that (a) the linear no along-track drift condition probably provides satisfactory results for formations up to at least 8 km in size; (b) the addition of the nonlinear terms without including the J_2^2 in the Hamiltonian provides some, but not substantial improvement; and (c) including the J_2^2 in the Hamiltonian provides much better results than not including them. It must be kept in mind that when using the nonlinear theory it may be necessary to include other zonal harmonics in the theory since they are of the same order of magnitude as the J_2^2 terms. This has not been done here, but is straightforward given the averaged Hamiltonian and using the approach presented herein. In addition, it should be noted that the long-periodic terms appear as secular terms of $\mathcal{O}(J_2^2)$ over a period of time much shorter than the perigee rotation period. Since the numerical procedure does not average over a long period of time, the computed δa would vary depending on which portion of the period was being calculated. The long-periodic terms are proportional to the eccentricity, and in this particular example $e = 0.01$; consequently, the effect would be very small.

8.3 DYNAMIC MODEL ERROR EFFECT COMPARISON

When designing control and navigation subsystems for a satellite formation, one of the key – and challenging – questions that must be answered is which relative motion theory should be used. The answer to this question is dependent on the reference, or chief, orbit, the size and type of the formation and the required accuracy of the state knowledge and control.

Numerous linear and nonlinear theories have been presented in the literature. The theories compared in this section are the CW and TH equations, discussed in Chapter 5; the GA theory [75], presented in Section 7.3; a small eccentricity version of the GA theory; and two nonlinear theories, the unit-sphere approach, presented in Section 7.1, and the Yan–Alfriend theory [123], discussed in the previous section. The equations for the small-eccentricity theory are given in Appendix G. To help the designer, this section presents a comparison of the errors that occur with various theories. However, the results should not be considered as a theory comparison, but as a comparison of the errors associated

Table 8.4 Theory comparison

Theory	Eccentricity	J_2	Nonlinearity
CW	$e = 0$	No	No
Lawden	$0 \leq e < 1$	No	No
Gim–Alfriend	$0 \leq e < 1$	Yes	No
Small e	$e \ll 1$	Yes	No
Unit sphere	$0 \leq e < 1$	Yes	Yes
Yan–Alfriend	$0 \leq e < 1$	Yes	Yes

with not modeling the effects of the chief eccentricity, J_2 and nonlinearities. Table 8.4 summarizes the effects modeled with these theories.

For comparing the effect of not modeling the various effects a modeling error index is introduced. This index does not require linearization of the equations of motion so nonlinear theories can also be evaluated. The index can be thought of as proportional to the percentage error, consequently the smaller the index the more accurate the theory. The two key parameters in the evaluation are the eccentricity of the reference orbit and the size measure of the relative motion orbit. This nonlinear index is a variation of one introduced by Junkins [151] for the comparison of linear theories.

Consider the nonlinear differential equations of motion

$$\dot{\mathbf{x}} = \mathbf{f}(\mathbf{x}, t), \quad \mathbf{x}(t_0) = \mathbf{x}_0 \tag{8.56}$$

Junkins [151] used as the nonlinearity index

$$\nu = \sup_{i=1,\ldots,N} \frac{\|\Phi_i\,(t, t_0) - \bar{\Phi}(t, t_0)\|}{\|\bar{\Phi}(t, t_0)\|} \tag{8.57}$$

where $\bar{\Phi}\,(t, t_0)$ is a state transition matrix that is obtained from Eq. (8.56) with the expected initial condition $\bar{x}(t, t_0)$; $\Phi\,(t, t_0)$ is a state transition matrix that is obtained from Eq. (8.56) with a worst-case distribution of initial conditions neighboring the expected initial conditions. For example, if the problem is a breakup or explosion, the worst-case initial conditions would be the points on the surface of the 3D ellipsoid of the relative velocity created by the breakup. This approach was used in Ref. [151] to compare the accuracy of three linear theories for a circular reference orbit: The CW equations, the linear theory using polar coordinates and one obtained from differential orbital elements. The objective was to determine which theory best captured the nonlinear effects. The comparison showed that differential orbital elements were the most accurate. The objective here is different; it is to evaluate the effect of the modeling error even when the theory is nonlinear, and to compare the accuracy of the theories for specific types of relative motion orbits. Thus, a modification of the Junkins nonlinearity index is needed. Let $\bar{\mathbf{x}}_i\,(t)$ be the solution for the initial condition $\bar{\mathbf{x}}_i\,(t_0)$ at the corresponding points and let $\mathbf{x}_i\,(t)$ be the solution for the model

being considered. These need not be linearized solutions. It is important that the states be in dimensionless variables or a weighting matrix used. Let $\mathbf{W}$ be a weighting matrix that non-dimensionalizes $\mathbf{x}$, that is

$$\mathbf{y} = \mathbf{W}\mathbf{x} \tag{8.58}$$

Now define

$$\nu = \max_{i=1,\ldots,N} \nu_i \tag{8.59}$$

$$\nu_i = \left(\frac{\bar{\mathbf{y}}_i^T \bar{\mathbf{y}}_i}{\mathbf{y}_i^T \mathbf{y}_i} - 1 \right) \tag{8.60}$$

Note that if there is only one state and we let $y_i = \bar{y}\,(1+\gamma)$ then $\nu = 2|\gamma|$. Therefore, the index is proportional to the percentage error.

The index provides a method for comparing the errors that occur for the various theories for a specific formation. As shown earlier, in the one-dimensional case the index is representative of twice the percentage error. In the n-dimensional case, the acceptable value for the index can only be determined by the acceptable errors for the mission. Many factors, such as time between thruster firings, allowable error growth and allowable error impact on the decision of which specific model to use. The method presented here only provides a guideline for determining the dynamic effects that need to be included in the model for a specific problem. Also, keep in mind that the index represents the maximum error over all the initial conditions for the PCO. For a specific formation, the index should be evaluated over the range of possible initial conditions.

There are formations for which the modeling errors are minimal. For example, because the differential J_2 effects are caused primarily by the inclination difference for small eccentric orbits, the effect of not modeling J_2 is small if there is no out-of-plane motion, or if the out-of-plane motion is caused by a right ascension difference. The differential eccentricity effect is caused by δe^2. Therefore, its effect for near-circular orbits is small, but for highly-eccentric orbits, such as MMS (cf. Section 1.7), it can have as much impact as the inclination difference.

The effect of the modeling error is a function of the relative motion orbit. For example, a differential inclination causes out-of-plane drift, so any relative motion orbit that does not have a differential inclination will experience different types of errors. For the theory comparison, we have chosen the PCO. This is one of the more stressing cases since it involves out-of-plane motion. Actually, the PCO does not exist if the chief eccentricity is not zero. However, by correctly choosing the initial conditions, a periodic orbit which is a deformed PCO can be found for a spherical Earth. Finding the initial conditions is not simple in Cartesian coordinates, but finding them is straightforward using differential orbital elements.

For the non-spherical Earth model, it is best to use mean elements because the angular rates are constant, which means that the constraints to minimize

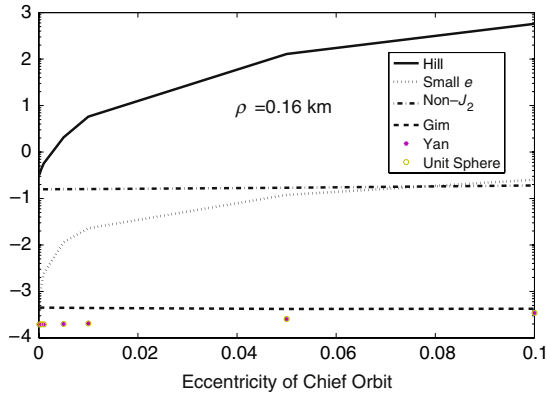

FIGURE 8.15 Index comparison for $\rho = 0.16$ km.

or prevent drift between the satellites are a function of only the momenta or (a, e, i). When including J_2, the differential elements given in Eq. (6.69) should be mean elements and as mentioned in Section 7.1, the $\delta a = 0$ is replaced by

$$\delta\bar{a} = -0.5 J_2 \bar{a}_0 \left(\frac{R_e}{\bar{a}_0}\right)^2 \left(\frac{3\bar{\eta}_0 + 4}{\bar{\eta}_0}\right) \times \left[\left(1 - 3\cos^2 \bar{i}_0\right) \frac{\bar{q}_{10}\delta\bar{q}_1 + \bar{q}_{20}\delta\bar{q}_2}{\bar{\eta}_0^2} + \delta\bar{i} \sin 2\bar{i}_0\right] \tag{8.61}$$

This constraint serves the same function with J_2 as $\delta a = 0$ does with no J_2; it negates the along-track drift. The derivation of Eq. (8.61) is discussed in more detail in Section 8.1.

The orbital elements of the chief used for the error effect evaluation are:

$$\bar{a}_0 = 8000 \text{ km}, \quad \bar{i}_0 = 50^\circ, \quad \bar{\Omega}_0 = \bar{\omega}_0 = \bar{M}_0 = 0 \tag{8.62}$$

First, consider the effect of the eccentricity of the reference orbit. Figures 8.15–8.17 show the effect of the modeling errors for the various models as a function of the chief eccentricity for PCO sizes of 0.16, 12 and 40 km, respectively. From these figures, the following conclusions are evident: (i) the CW equations are inaccurate, even for a small chief eccentricity. The index increases quickly and at $\bar{e}_0 = 0.1$ is almost two orders of magnitude greater than the index for the non-J_2 theory (TH equations); (ii) not including J_2 has a significant effect. The index for the TH equations is more than two orders of magnitude larger than that for the GA theory. In fact, the small e theory that includes first-order eccentricity effects in the non-J_2 terms and assumes $\bar{e}_0 = 0$ in the J_2 terms is more accurate than TH equations until $\bar{e}_0 \approx 0.06$; (iii) the unit sphere and the Yan–Alfriend nonlinear theories provide equivalent accuracy, although the two theories are different. The Yan-Alfriend theory includes J_2^2 terms, and by virtue of using orbital elements and the expansion in powers of J_2, includes nonlinear

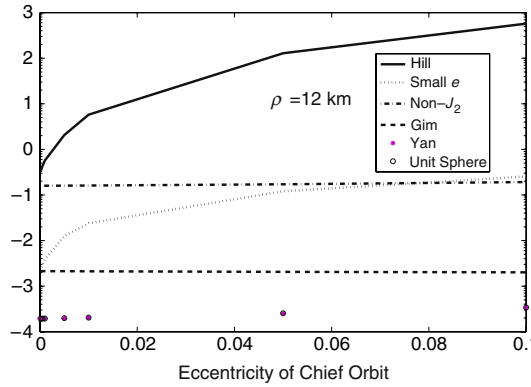

FIGURE 8.16 Index comparison for $\rho = 12$ km.

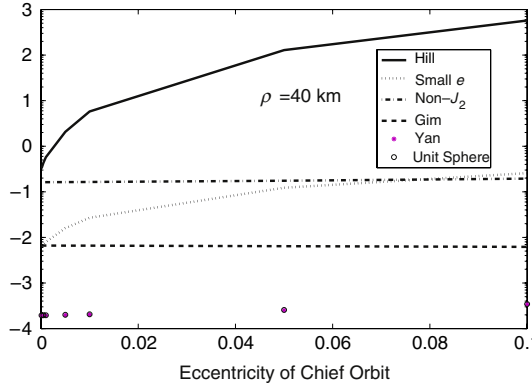

FIGURE 8.17 Index comparison for $\rho = 40$ km.

effects. By mapping the relative motion onto the unit sphere, the unit-sphere method better models the nonlinear effects, but does not include J_2^2 effects. These differences appear to balance each other, and result in the equivalent accuracy seen for the investigated examples.

Figures 8.18–8.20 show the effect of the modeling errors for the various models as a function of formation size for chief eccentricities of 0.001, 0.01 and 0.1, respectively. From these figures the following conclusions are evident. (i) The errors caused by not including the chief eccentricity and J_2 in the CW equations dominate any error caused by the linearization. The index is flat for formations up to 160 km in size. (ii) The errors caused by not including J_2 in the TH equations dominate any error caused by the linearization. The index is flat for formations up to 160 km in size, but smaller than the index for the CW equations because the chief eccentricity is included in the model. (iii) The unit sphere and Yan–Alfriend nonlinear theories provide equivalent accuracy. (iv) Even though $\nu < 0.01$ for the GA theory, for formation sizes less than 40 km it is still an order of magnitude larger than the nonlinear theories.

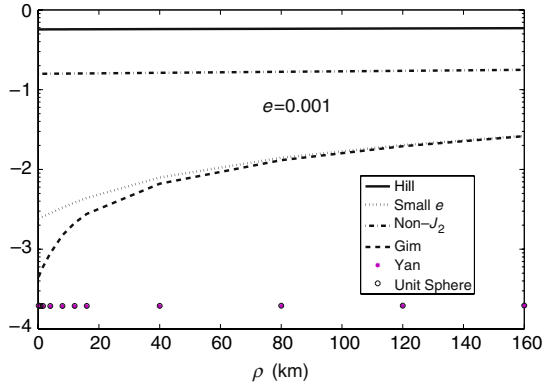

FIGURE 8.18 Index comparison for $e = 0.001$.

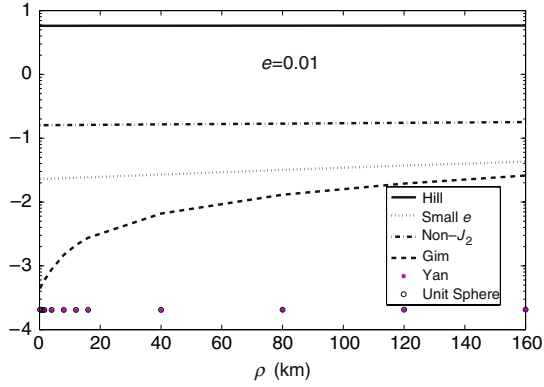

FIGURE 8.19 Index comparison for $e = 0.01$.

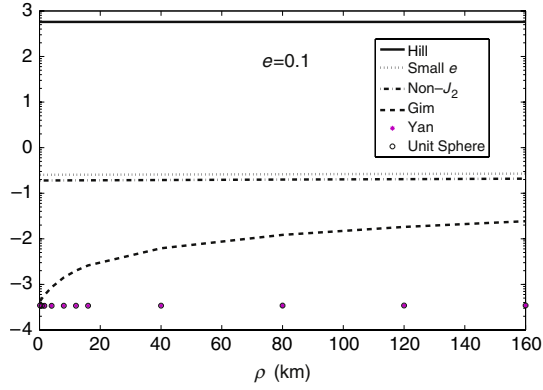

FIGURE 8.20 Index comparison for $e = 0.1$.

The properties of the perturbed relative orbit, under the no along-track drift constraint, are developed further in the following sections. The initial conditions on the differential orbital elements for the PCO relative orbit are related to its shape and size parameters. Furthermore, a basis for designing an intelligent control law for formation maintenance and *fuel balancing* is presented by exploiting the properties of the natural relative motion. We will use the classical orbital element representation in the rest of this chapter.

8.4 PERTURBED FUNDAMENTAL FREQUENCIES FOR FORMATIONS IN NEAR-CIRCULAR ORBITS

The *fundamental frequency* of the unperturbed periodic relative motion in the two-body problem is the mean motion of the chief (or the deputy). In general, the in-plane and cross-track fundamental frequencies are not the same for perturbed relative motion, due to perigee rotation and nodal precession. Knowledge of the perturbed frequencies due to J_2 aids in the design and tuning of the controllers for mitigating its adverse effects efficiently. The perturbations of the in-plane and cross-track frequencies associated with formations in near-circular orbits is treated in this section [139].

The linearized relative motion equations expressed in terms of the differential orbital elements were derived in Section 7.1. Inspection of Eq. (7.18) reveals that in the absence of differential nodal precession, the fundamental cross-track frequency is $\dot{\lambda}_1 = \dot{M}_1 + \dot{\omega}_1$, the rate of change of the mean argument of latitude of the deputy. This is no longer true if $\delta\dot{\Omega} \neq 0$. Equations (7.16)–(7.17) can be simplified further by expanding r and θ to first-order in eccentricity and neglecting terms involving frequencies $2M$ and higher:

$$r \approx a(1 - e\cos M) \tag{8.63}$$

$$\theta \approx \omega + M + 2e\sin M \tag{8.64}$$

$$\sin\theta \approx \sin\lambda - e\sin\omega \tag{8.65}$$

$$\cos\theta \approx \cos\lambda - e\cos\omega \tag{8.66}$$

For orbits with small eccentricities and even for small formations, δM and $\delta\omega$ can be large, but $\delta\lambda$ remains small. Substitution of Eqs. (8.63)–(8.66) in Eqs. (7.16)–(7.18) results in

$$x \approx \delta a + a_0[(e_1\sin\delta M)\sin M_0 + (e_0 - e_1\cos\delta M)\cos M_0] \tag{8.67}$$

$$\begin{aligned} y \approx\ & a_0[\delta\lambda + \delta\Omega\cos i_0 - e_0(e_1\sin\delta M)] \\ & + 2a_0[-(e_0 - e_1\cos\delta M)\sin M_0 + (e_1\sin\delta M)\cos M_0] \end{aligned} \tag{8.68}$$

$$z \approx a_0\left[\delta i\sin\lambda_0 - \sin i_0\delta\Omega\cos\lambda_0 - \frac{3}{2}e_0(\delta i\sin\omega_0 - \sin i_0\delta\Omega\cos\omega_0)\right] \tag{8.69}$$

It has been shown previously in Eq. (8.15) that δa, appearing in Eq. (8.67), is required to be $\mathcal{O}(J_2)$ for preventing along-track secular drift [143]. Equations (8.67)–(8.69) reveal, upon further analysis, the frequencies of motion and a means to set up the initial conditions for formations in near-circular orbits.

8.4.1 In-plane and cross-track frequencies

The analysis to follow is based on the mean orbital elements. At this point, the secular drift rates $\delta\dot{\lambda}$ and $\delta\dot{\Omega}$ can be substituted into Eqs. (8.67)–(8.68) to obtain

$$x \approx \delta a + \rho_x \sin(M_0 + \alpha_x) \tag{8.70}$$

$$\begin{aligned} y \approx\ & a_0[\delta\lambda(0) + \delta\Omega(0)\cos i_0 - e_0(e_1 \sin \delta M(0))] \\ & + a_0[\delta\dot{\lambda} + \delta\dot{\Omega}\cos i_0]t + 2\rho_x \cos(M_0 + \alpha_x) \end{aligned} \tag{8.71}$$

where

$$\rho_x = a_0\sqrt{(e_1 \sin \delta M)^2 + (e_0 - e_1 \cos \delta M)^2} \tag{8.72}$$

is the amplitude of the radial periodic motion and

$$\alpha_x = -\frac{\pi}{2} + \tan^{-1}\left[-\frac{e_1 \sin \delta M}{e_0 - e_1 \cos \delta M}\right] \tag{8.73}$$

is the in-plane phase angle. Equations (8.72)–(8.73) show that for circular reference orbits, $\rho_x = a_0 e_1$ is a constant and $\alpha_x = -\frac{\pi}{2} + \delta M$. Hence, since $\delta M = \delta M(0) + \delta\dot{M}t$, the in-plane frequency is $n_{xy} = \dot{M}_0 + \delta\dot{M} = \dot{M}_1$, the mean motion of the deputy. For small formations, the differential inclination itself is $\mathcal{O}(J_2)$. Hence, the approximation

$$n_{xy} \approx \dot{M}_0 \tag{8.74}$$

is valid.

Equation (8.69) can also be represented as follows:

$$z \approx \rho_z \sin(\lambda_0 + \alpha_z) - \frac{3}{2}\rho_z e_0 \sin(\omega_0 + \alpha_z) \tag{8.75}$$

where

$$\rho_z \approx a_0\sqrt{\delta i^2 + \sin^2 i_0(\delta\Omega(0) + \delta\dot{\Omega}t)^2} \tag{8.76}$$

and

$$\alpha_z = \tan^{-1}\left[-\frac{\sin i_0(\delta\Omega(0) + \delta\dot{\Omega}t)}{\delta i}\right] \tag{8.77}$$

It can be shown by differentiating Eq. (8.77) that

$$\dot{\alpha}_z = \frac{-\sin i_0 \delta\dot{\Omega}\delta i}{\delta i^2 + (\sin i_0 \delta\Omega)^2} \tag{8.78}$$

As can be seen from the above equation, $\dot{\alpha}_z$ is not a constant due to the action of differential nodal precession. However, focusing attention on a relatively

small time-scale and ignoring the effect of $\delta\dot{\Omega}$ in the denominator of the above equation, an estimate of the rate of change of the phase angle is

$$\dot{\alpha}_z \approx \frac{-\sin i_0 \delta\dot{\Omega}\delta i}{\delta i^2 + (\sin i_0 \delta\Omega(0))^2} \tag{8.79}$$

The above analysis shows that the cross-track natural frequency, n_z, can be approximated as

$$n_z \approx \dot{M}_0 + \dot{\omega}_0 - \frac{\sin i_0 \delta\dot{\Omega}\delta i}{\delta i^2 + (\sin i_0 \delta\Omega(0))^2} \tag{8.80}$$

The result presented above is accurate to $\mathcal{O}(J_2)$ and valid for near-circular orbits, over a finite period of time ($\approx$ 1 day).

8.5 SELECTION OF THE PCO INITIAL CONDITIONS FOR NEAR-CIRCULAR ORBITS

The procedures for determining the initial conditions for perturbed PCO and GCO have been presented in Refs. [152,153] and also in Eqs. (6.69). The development herein utilizes the approximate solutions to the relative motion variables given by Eqs. (8.67)–(8.69), which are valid for near-circular orbits. The along-track and cross-track initial conditions for a PCO can be parameterized as

$$y(0) = \rho(0)\cos(\lambda_0(0) + \alpha(0)) \tag{8.81}$$

$$z(0) = \rho(0)\left[\sin(\lambda_0(0) + \alpha(0)) - \frac{3}{2}e_0 \sin(\omega_0 + \alpha(0))\right] \tag{8.82}$$

where $\alpha(0)$ is the desired initial phase angle and $\rho(0)$ is the initial radius of the PCO, in the yz plane. Note that Eqs. (8.81) and (8.82) are valid at the initial time and do not describe the ensuing motion. Hence, the same initial phase angle is used for $y(0)$ and $z(0)$. Upon comparing Eq. (8.71) with Eq. (8.81) and similarly, Eq. (8.75) with Eq. (8.82), it is observed that $\rho_x = 0.5\rho(0)$ and $\rho_z = \rho(0)$.

The initial differential orbital elements satisfying the conditions of Eqs. (8.81)–(8.82) can be obtained from Eqs. (8.68)–(8.69) as

$$\delta\lambda(0) + \delta\Omega(0)\cos i_0 = \frac{\rho(0)e_0}{2a_0}\cos(\omega_0(0) + \alpha(0)) \tag{8.83}$$

$$e_1 \sin\delta M(0) = \frac{\rho(0)}{2a_0}\cos(\omega_0(0) + \alpha(0)) \tag{8.84}$$

$$e_1 \cos\delta M(0) = e_0 - \frac{\rho(0)}{2a_0}\sin(\omega_0(0) + \alpha(0)) \tag{8.85}$$

$$\delta\Omega(0) = -\frac{\rho(0)}{a_0 \sin i_0}\sin\alpha(0) \tag{8.86}$$

$$\delta i = \frac{\rho(0)}{a_0}\cos\alpha(0) \tag{8.87}$$

Equations (8.83)–(8.87) do not contain small divisors, except for the case of equatorial orbits. An eccentricity-induced bias term is present in the RHS of Eq. (8.83). Equations (8.84) and (8.85) provide a means to calculate e_1 and $\delta M(0)$, thus enabling the computation of $\delta e = e_1 - e_0$. For circular orbits, $\delta e(0) = \rho(0)/(2a_0)$ and $\tan(\delta M(0)) = -\cot(\omega_0(0) + \alpha(0))$. Finally, $\delta\lambda(0)$ can be determined from Eqs. (8.86) and (8.83). The required change in the semimajor axis is obtained from the no along-track constraint, Eq. (8.15).

Example 8.2. *Consider the example of setting up of the PCOs with the following mean orbital elements of the chief:*

$$\begin{aligned} a_0 = 7092\ \text{km}, \quad e_0 = 0, \quad i_0 = 70^\circ \\ \Omega_0 = 45^\circ, \quad \omega_0 = 0^\circ, \quad M_0 = 0^\circ \end{aligned} \tag{8.88}$$

The initial conditions of the deputy for the example mean elements of the chief are obtained from Eqs. (8.83)–(8.87) and Eq. (8.15). Evolutions of four PCOs, with $\rho = 1$ km and $\alpha(0)$ values ranging from 0° to 90°, are shown in Fig. 8.21 for 50 orbits of the chief. The relative orbits do remain bounded along the y-axis, but also present in each figure, to varying extents, is secular growth along the z-axis and precession, due to non-commensurate in-plane and out-of-plane frequencies. Note also the variations of the precession patterns for different values of $\alpha(0)$. The evolution of the error in the radius of the PCO for a deputy with $\alpha(0) = 0$ is shown over ten orbital periods of the chief in Fig. 8.22. The secular error over this period reaches approximately 45 m, i.e., the rate of growth is 4.5 m/orbit.

For circular reference orbits, the first-order differential drift rates are functions of δa and δi:

$$\delta\dot{\lambda} = \frac{\partial\dot{\lambda}}{\partial a}\delta a + \frac{\partial\dot{\lambda}}{\partial i}\delta i \tag{8.89a}$$

$$\delta\dot{\Omega} = \frac{\partial\dot{\Omega}}{\partial i}\delta i \tag{8.89b}$$

and they can be evaluated by using the following partial derivatives:

$$\frac{\partial\dot{\lambda}}{\partial i} = -6Jn_0 \sin 2\bar{i}_0 \tag{8.90a}$$

$$\frac{\partial\dot{\lambda}}{\partial a} = -\frac{3n_0}{2\bar{a}_0} \tag{8.90b}$$

$$\frac{\partial\dot{\Omega}}{\partial i} = \frac{3}{2}Jn_0 \sin\bar{i}_0 \tag{8.90c}$$

where J is as defined in Section 7.5. Even though the mean elements of the chief are used in the partial derivatives shown in Eq. (8.90), these equations are valid for estimating the differential drift rates of the deputies as well, since a first-order approximation is being adopted.

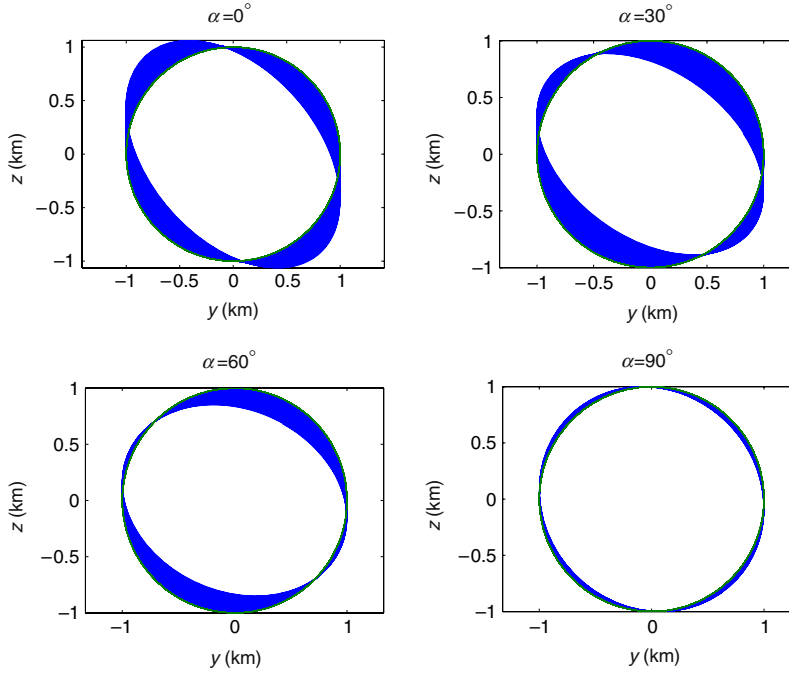

FIGURE 8.21 Uncontrolled PCOs for various $\alpha(0)$ values (50 orbits shown).

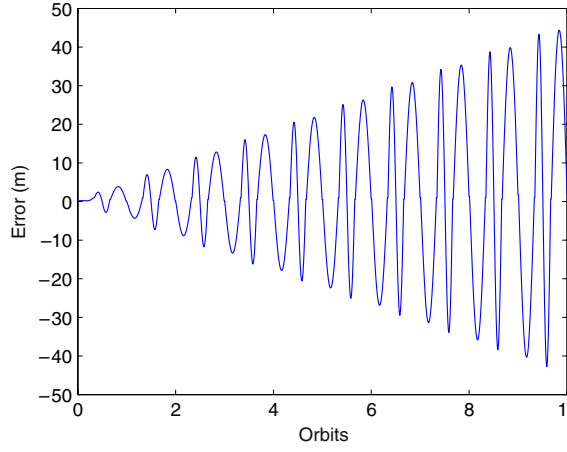

FIGURE 8.22 Evolution of the error in the radius of the PCO for an uncontrolled satellite with $\alpha(0) = 0$.

8.6 MATCHING THE IN-PLANE AND CROSS-TRACK FUNDAMENTAL FREQUENCIES

A mismatch between the in-plane and cross-track frequencies causes precession of the relative orbit, which may not be desirable for some applications. The

condition under which the two frequencies are equal is derived in this section. Equations (8.74) and (8.80) show that the difference between the in-plane and cross-track frequencies, over a short time interval (compared to the period of the differential nodal precession rate) is

$$n_z - n_{xy} = \dot{\omega}_0 - \frac{\delta\dot{\Omega}\delta i \sin i_0}{\delta i^2 + (\delta\Omega(0)\sin i_0)^2} \tag{8.91}$$

The rates of perigee rotation and differential nodal precession, valid for circular orbits, can respectively, be written as

$$\dot{\omega}_0 = -k\left(2 - \frac{5}{2}\sin^2 i_0\right) \tag{8.92}$$

and

$$\delta\dot{\Omega} = -k \sin i_0 \delta i \tag{8.93}$$

where

$$k = -1.5 J_2 \left(\frac{R_e}{a_0}\right)^2 n_0 \tag{8.94}$$

Thus, the frequency mismatch is estimated to be

$$n_z - n_{xy} = k \sin^2 i_0 \left(\frac{5}{2} + \frac{\delta i^2}{\delta i^2 + (\delta\Omega(0)\sin i_0)^2}\right) - 2k \tag{8.95}$$

For the special case of the PCO, substitution of Eqs. (8.86)–(8.87) into Eq. (8.95) leads to the following result:

$$i_0^* = \sin^{-1}\left(\sqrt{\frac{2}{2.5 + \cos^2\alpha(0)}}\right) \tag{8.96}$$

Thus, the frequency-matching condition is satisfied by two possible values of the chief's orbit inclination for any $\alpha(0)$. The inclinations for $\alpha(0) = 0$ are $i_0^* = 49.11°$ and 130.89°and those for $\alpha(0) = 90°$ are the critical inclination values: $i_0^* = 63.43°$ and 116.57°. The numerical results presented in Refs. [154, 155] agree very closely with the special inclination values determined above.

Figure 8.23 shows 15 relative motion orbits for a 7100 km circular reference orbit with $\alpha(0) = 0$ and $i_0 = 49.11°$. The effect of the frequency-matching condition is apparent from a comparison of Fig. 8.23 and Fig. 8.21. The mismatch in the in-plane and cross-track frequencies results in the precession of the PCO shown in Fig. 8.21. If allowed to continue in this manner indefinitely, without control, the PCO of Fig. 8.23 will also distort significantly due to the effect of differential nodal precession.

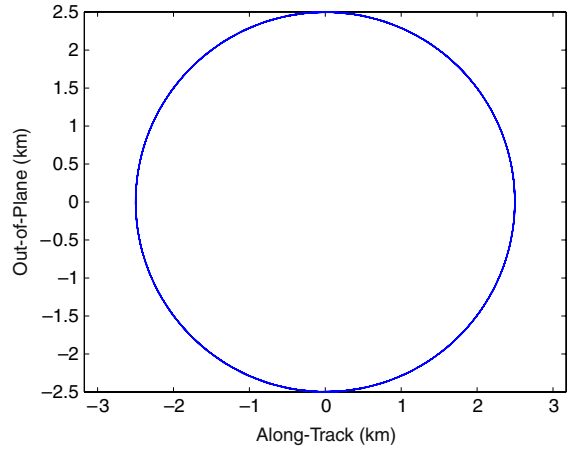

FIGURE 8.23 Frequency matched relative orbits for $i_0 = 49.11°$ (15 orbits).

It can be shown by substituting Eq. (8.93) into Eq. (8.79) and from Eqs. (8.86)–(8.87) that for a PCO formation, the natural rate of change of the cross-track phase angle as a function of its initial phase angle is given by

$$\dot{\alpha}_z = k \sin^2 i_0 \cos^2 \alpha(0) \tag{8.97}$$

Considering an infinite number of satellites distributed in a PCO ($\alpha(0) \in [0, 2\pi]$), the average rate of change of the phase angle can be obtained as

$$(\dot{\alpha}_z)_{ave} = \frac{1}{2} k \sin^2 i_0 \tag{8.98}$$

Note that $\dot{\alpha}_z$ and $(\dot{\alpha}_z)_{ave}$ do not depend on the size of the relative orbit.

8.6.1 Amplitude considerations

This section treats the effects of the parameters, i_0 and $\alpha(0)$ on the cross-track amplitude growth-rate. The in-plane amplitude variation is negligible, as long as Eq. (8.15) is satisfied.

Equation (8.76) can be expressed directly in terms of i_0 and $\alpha(0)$ via Eqs. (8.86), (8.87), and (8.93). The result obtained is

$$\rho_z \approx \rho \sqrt{1 + k^2 t^2 \sin^4 i_0 \cos^2 \alpha(0) + kt \sin^2 i_0 \sin 2\alpha(0)} \tag{8.99}$$

Equation (8.99) shows that for non-equatorial orbits, cross-track amplitude growth rate is zero for the special case: $\alpha(0) = 90°, 270°$ or equivalently, for $\delta i = 0$. Another special case of zero linear-growth is obtained, corresponding to $\alpha(0) = 0, 180°$, by neglecting the t^2 term in Eq. (8.99). This assumption is reasonable for a time period of one day. Equations (8.96)–(8.99), together,

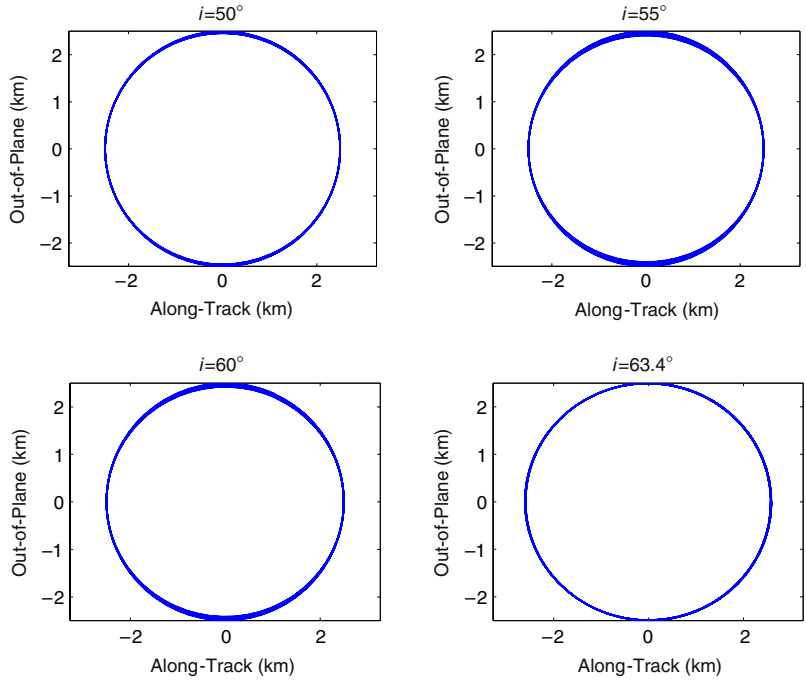

FIGURE 8.24 Non-precessing relative orbits for various inclinations (15 orbits shown for each inclination).

explain the existence of the so-called "magic inclinations" for obtaining non-precessing or "frozen" relative orbits [154,155].

Relative orbits for other values of i_0, set up with the corresponding values of $\alpha(0)$ given by Eq. (8.96), are shown in Fig. 8.24. The orbits in these figures do not precess, but show localized, cross-track growth for inclinations corresponding to $\alpha(0) \neq 0, 90°$.

8.7 PCO FORMATION MAINTENANCE BASED ON THE MODIFIED CW EQUATIONS

In this section, expressions for the components of the J_2-induced perturbing acceleration vector are derived for circular orbits ($e_0 = 0$) by retrofitting a modified set of CW equations to the analytical solutions given by Eqs. (8.67)–(8.69). This objective is achieved by differentiating each of Eqs. (8.67)–(8.69) twice, while holding δa, δe, and δi constant. Furthermore, since δa is $\mathcal{O}(J_2)$, the term $\dot{M}_0^2 \delta a$ is approximated by $n_0^2 \delta a$ where n_0 is the unperturbed two-body mean motion of the chief. The results are

$$\ddot{x} - 2\dot{M}_0 \dot{y} - 3\dot{M}_0^2 x = -3n_0^2 \delta a - 2n_0 a_0 \left(\delta\dot{\lambda} + \delta\dot{\Omega}\cos i_0\right) \tag{8.100a}$$

$$\ddot{y} + 2\dot{M}_0 \dot{x} = 0 \tag{8.100b}$$

$$\ddot{z} + \dot{\lambda}_0^2 z = 2a_0 \dot{\lambda}_0 \delta\dot{\Omega} \sin i_0 \sin \lambda_0 \tag{8.100c}$$

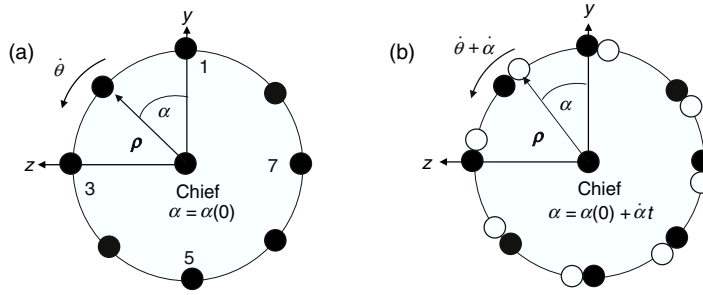

FIGURE 8.25 (a) PCO formation with $\alpha = \alpha(0)$ when the chief is at the ascending node. (b) PCO formation with $\alpha = \alpha(0) + \dot{\alpha}t$ when the chief is at the ascending node.

The terms involving $\delta\ddot{\Omega}$ and $\delta\ddot{\lambda}$ have been neglected in Eqs. (8.100). The secular variation of $\delta\dot{\Omega}$ can also be incorporated into these equations. The control magnitude required for PCO formation maintenance is $\rho n_0^2 \mathcal{O}(J_2)$. Hence, neglecting terms of $\mathcal{O}(J_2^2)$, Eqs. (8.100) can be modified as

$$\ddot{x} - 2\dot{M}_0\dot{y} - 3\dot{M}_0^2 x = -3n_0^2\delta a + u_{x_c} \tag{8.101a}$$

$$\ddot{y} + 2\dot{M}_0\dot{x} = u_{y_c} \tag{8.101b}$$

$$\ddot{z} + \dot{M}_0^2 z = -2n_0\dot{\omega}_0 z - 2\rho(0)kn_0 \sin i_0^2 \sin\lambda_0 \cos\alpha(0) + u_{z_c} \tag{8.101c}$$

where u_{x_c}, u_{y_c}, and u_{z_c} are the control accelerations along their respective axes.

An impractical alternative for formation maintenance in the presence of the J_2-perturbation is to cancel its effect by the application of thrust. A better approach is to use a control-induced formation phase rotation rate $\dot{\alpha}$ of $\mathcal{O}(J_2)$, instead of enforcing the CW-result: $\alpha = \alpha(0)$. The additional benefit of inter-satellite fuel balancing due to such a scheme has been demonstrated in Refs. [139,153,156]. In essence, this scheme modifies the disturbance term of Eq. (8.101c) by requiring the PCO differential orbital elements of Eqs. (8.83)–(8.87) to depend on a time-varying phase angle, given by $\alpha = \alpha(0) + \dot{\alpha}t$. The result of this modification is shown pictorially in Fig. 8.25. Figure 8.25(a) shows the snapshot of the ideal PCO formation when the chief is at the ascending node. Deputies 1 and 5 have the maximum δi and $\delta\Omega = 0$, whereas deputies 3 and 7 have the maximum $\delta\Omega$ and $\delta i = 0$. Hence, deputies 1 and 5 will require the maximum fuel to mitigate the effects of differential nodal precession and the pair 3 and 7 will require the least fuel for orbit maintenance. Figure 8.25(b) shows that the effect of the formation phase rotation is to perturb the orbit rates of all the deputies ever so slightly so that they appear as shown by the small white circles at a subsequent ascending nodal crossing of the chief. As this process progresses over time, gradually, each deputy will spend equal time in "good" and "bad" locations, thereby balancing the fuel required for formation maintenance among the deputies. Another alternative for fuel balancing using the virtual center approach is discussed in Refs. [5,7].

Therefore, the following reference trajectories are selected to estimate the control requirements for formation maintenance:

$$x_r(t) = 0.5\rho(0)\sin(\lambda_0(0) + \alpha(0) + (\dot{M}_0 + \dot{\alpha})t) + \delta a \tag{8.102}$$

$$y_r(t) = \rho(0)\cos(\lambda_0(0) + \alpha(0) + (\dot{M}_0 + \dot{\alpha})t) \tag{8.103}$$

$$z_r(t) = \rho(0)\sin(\lambda_0(0) + \alpha(0) + (\dot{M}_0 + \dot{\alpha})t) \tag{8.104}$$

The choice of the frequency, $\dot{M}_0$, in Eqs. (8.102)–(8.104) is not unique. Perigee rotation of the chief can also be accounted for in the reference orbit. However, this ambiguity in the choice of the reference frequency can also be resolved by absorbing $\dot{\omega}$ into $\dot{\alpha}$. The natural motion variables, as given by Eqs. (8.70), (8.71), and (8.75), differ from their respective reference trajectories given by Eqs. (8.102)–(8.104). Hence, control inputs are required for trajectory following.

The control accelerations obtained by substituting Eqs. (8.102)–(8.104) into Eqs. (8.101) are

$$u_{x_c} \approx \rho(0)n_0\dot{\alpha}\sin(\lambda_0(0) + \alpha(0) + (\dot{M}_0 + \dot{\alpha})t) \tag{8.105}$$

$$u_{y_c} \approx -\rho(0)n_0\dot{\alpha}\cos(\lambda_0(0) + \alpha(0) + (\dot{M}_0 + \dot{\alpha})t) \tag{8.106}$$

$$\begin{aligned} u_{z_c} \approx\ & 2n_0(\dot{\omega}_0 - \dot{\alpha})\rho(0)\sin(\lambda_0(0) + \alpha(0) + (\dot{M}_0 + \dot{\alpha})t) \\ & + 2\rho(0)kn_0\sin^2 i_0\cos(\alpha(0))\sin\lambda_0 \end{aligned} \tag{8.107}$$

Eqs. (8.105)–(8.106) indicate that the magnitudes of the in-plane thrust acceleration components for formation maintenance depend linearly on $\dot{\alpha}$. Further insight on the dependence of the cross-track control acceleration magnitude on $\dot{\alpha}$ is obtained by squaring Eq. (8.107) and averaging the result over an orbit of the chief, thereby eliminating the short-periodic variations. The mean square cross-track control acceleration is given below:

$$u_{z_c}^2 = 2\rho^2(0)n_0^2\left[(\dot{\omega}_0 - \dot{\alpha} + k\sin^2 i_0)^2\cos^2(\alpha(0)) + (\dot{\omega}_0 - \dot{\alpha})^2\sin^2\alpha(0)\right] \tag{8.108}$$

The minimum value of $u_{z_c}^2$ is obtained for

$$\dot{\alpha} = \dot{\omega}_0 + k\sin^2 i_0\cos^2\alpha(0) = \dot{\omega}_0 + \dot{\alpha}_z \tag{8.109}$$

This is not a surprising result, considering the expression for the natural cross-track phase angle rotation rate provided by Eq. (8.97). For an orbit with inclination satisfying Eq. (8.96), the optimal control-induced phase rotation rate is zero, since $\dot{\omega}_0 = -\dot{\alpha}_z$. Therefore, orbit control is not required for such a satellite, at least over a period of one day.

8.7.1 Formation maintenance without radial thrust

An important special case of control without the use of radial thrust is examined next. Successive differentiations of the in-plane equations and imposition of the

zero-radial thrust condition result in the following:

$$\dddot{y} + \dot{M}_0^2 \ddot{y} = \ddot{u}_{y_c} - 3\dot{M}_0^2 u_{y_c} \tag{8.110}$$

Substitution of Eq. (8.103) into Eq. (8.110) results in the following:

$$u_{x_c} = 0 \tag{8.111}$$

$$u_{y_c} = -0.5 n_0 \rho(0) \dot{\alpha} \cos(\lambda_0(0) + \alpha(0) + (\dot{M}_0 + \dot{\alpha})t) \tag{8.112}$$

$$x(t) = 0.5 \left(1 + \frac{0.5\dot{\alpha}}{n_0}\right) \rho(0) \sin(\lambda_0(0) + \alpha(0) + (\dot{M}_0 + \dot{\alpha})t) + x_{bias} \tag{8.113}$$

where, as will be shown in Chapter 10, x_{bias} is a constant, related to δa. In the absence of radial thrust, $x(t)$ does not follow the reference solution of Eq. (8.102) exactly. A comparison of Eqs. (8.111)–(8.112) with Eqs. (8.105)–(8.106) shows a 50% reduction in the net in-plane thrust acceleration achieved by not using radial thrust and relaxing the tracking requirement for the radial component of motion. The difference between the two expressions in Eq. (8.113) and Eq. (8.102) is $\mathcal{O}(J_2)$.

8.8 FUEL MINIMIZATION AND BALANCING

Balancing the rate of fuel-consumption among identical satellites in a formation results in a common ballistic coefficient (cf. Section 1.3.4) for all the satellites. In the absence of radial thrust, the mean square control acceleration, averaged over an orbit, can be evaluated as shown below:

$$\mathcal{J} = \frac{n_0}{2\pi} \int_0^{2\pi/n_0} (u_{y_c}^2 + u_{z_c}^2) \mathrm{d}t \tag{8.114}$$

The performance index defined above simplifies the analysis, but it does not accurately represent the fuel requirement. However, $\mathcal{J}$ is directly proportional to the fuel consumption for power-limited, low-thrust propulsion. Substituting Eqs. (8.107) and (8.112) into Eq. (8.114) and evaluating the integral gives

$$\mathcal{J} = (\rho n_0)^2 \left[\frac{1}{8}\dot{\alpha}^2 + 2(\dot{\alpha} - \dot{\omega}_0)^2 + 2k^2 \sin^4 i_0 \cos^2 \alpha(0) \right.$$
$$\left. - 4(\dot{\alpha} - \dot{\omega}_0) k \sin^2 i_0 \cos^2 \alpha(0) \right] \tag{8.115}$$

The averaged cost per satellite, considering an infinite number of satellites over an orbit of the chief, can be represented as

$$\mathcal{J}_{Formation} = \frac{n_0}{4\pi^2} \int_0^{2\pi/n_0} \int_0^{2\pi} (u_{y_c}^2 + u_{z_c}^2) \mathrm{d}\alpha(0) \mathrm{d}t \tag{8.116}$$

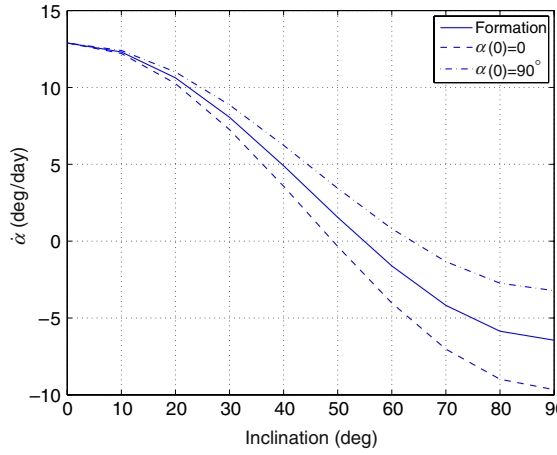

FIGURE 8.26 Optimal phase rotation rate as a function of inclination.

Evaluation of the integral Eq. (8.116) results in

$$\mathcal{J}_{Formation} = (\rho n_0)^2 \left[\frac{1}{8}\dot{\alpha}^2 + 2(\dot{\alpha} - \dot{\omega}_0)^2 + k^2 \sin^4 i_0 - 2(\dot{\alpha} - \dot{\omega}_0) k \sin^2 i_0 \right] \tag{8.117}$$

Minimization of the above expression with respect to $\dot{\alpha}$ yields

$$\dot{\alpha}_{opt_{Formation}} = \frac{16}{17}\left(\dot{\omega}_0 + \frac{1}{2}k \sin^2 i_0\right) = \frac{16}{17}(\dot{\omega}_0 + \dot{\alpha}_{z_{ave}}) \tag{8.118}$$

Note that the results of Eqs. (8.94) and (8.98) have been used in the derivation of Eq. (8.118). For each deputy in the formation, the optimal phase rotation rate as a function of its initial phase angle is given by

$$\dot{\alpha}_{opt_{Satellite}} = \frac{16}{17}(\dot{\omega}_0 + k \sin^2 i_0 \cos^2 \alpha(0)) = \frac{16}{17}(\dot{\omega}_0 + \dot{\alpha}_z) \tag{8.119}$$

Equations (8.119) and (8.109) are closely related. Whereas the result of Eq. (8.109) is obtained by minimizing the cross-track thrust acceleration only, the result of Eq. (8.119) minimizes the total cost. Hence, the optimal value of $\dot{\alpha}$ is dictated predominantly by the cross-track dynamics. The optimal rate of phase shift for a formation is independent of the radius of the relative orbit and it is $\mathcal{O}(J_2)$.

Figure 8.26 shows the variation of $\dot{\alpha}$ for a formation as well as two individual satellites, one with $\alpha(0) = 0$ and the other with $\alpha(0) = 90°$. There exist multiple i_0 and $\alpha(0)$ pairs satisfying Eq. (8.96) for which $\dot{\alpha} = 0$ is optimal. For a formation $\dot{\alpha} = 0$ if $i_0 = 54.73°$ or its supplement, the values for which the perturbed mean motion is equal to the two-body mean motion. For such a formation, $\dot{\omega}_0$ is equal and opposite $\dot{\alpha}_{z_{ave}}$.

The costs for individual satellites, as well as the average formation maintenance cost, can also be minimized with respect to inclination. Simultaneous minimization of $\mathcal{J}$, given by Eq. (8.115), with respect to i_0 and $\alpha(0)$, results in the following special relationship for the inclination:

$$i_0^{**} = \sin^{-1}\left(\sqrt{\frac{20 + 8\cos^2\alpha(0)}{88\cos^2\alpha(0) - 64\cos^4\alpha(0) + 25}}\right) \tag{8.120}$$

Equation (8.120) shows that for a satellite with $\alpha(0) = 0$, $i_0^{**} = i_0^{*} = 49.11°$. Similarly, the critical inclination value is optimal for a satellite with $\alpha(0) = 90°$. The value of i_0^{**} for a formation can be obtained from Eqs. (8.117)–(8.118), or directly, by substituting in Eq. (8.120), $\cos^2\alpha(0) = 0.5$. The result is $i_0^{**} = 42.3°$.

Control acceleration for formation-keeping with respect to the reference trajectory chosen is required to mitigate two effects: frequency mismatch and cross-track amplitude variation. The i_0-$\alpha(0)$ constraint given by Eq. (8.96) automatically accounts for the first effect, but not the second. Equations (8.96) and (8.120) are simultaneously satisfied by $i_0 = 49.11°$ and the critical inclination.

SUMMARY

In mean-element space, the Hamiltonian is a function of only the momenta, i.e., the angles are ignorable coordinates. This means that the angle rates are functions of only the momenta, and are therefore constant. Thus, one can analytically investigate the effect of the momenta differences and initial angle values on the design and maintenance of formations. This fact led to three important developments presented in this section.

Firstly, the design of relative motion orbits is more straightforward in mean-element space. It is analogous to the design of formations in orbital element space for a spherical Earth. The differential inclination, differential eccentricity and differential initial right ascension define the size of the formation, and the differential mean anomaly and argument of perigee define the phasing and center location of the formation. One then transforms the mean elements to osculating elements to obtain the initial position and velocity.

Secondly, constraints for minimizing the drift in the angles resulting from the J_2 perturbation were derived and demonstrated by simulation. These are constraints on the mean differential momenta, or $(\delta a, \delta a, \delta e)$. To minimize the along-track drift in the presence of the J_2 perturbation, an analytical expression for a semimajor axis difference was derived. This constraint should always be used as it does not impact on the formation design just as the $\delta a = 0$ constraint does not impact on the formation design for a spherical Earth. For a formation of approximately 1 km in size, this semimajor axis difference is typically only a few meters.

In addition, analytical expressions for negating the differential nodal precession or differential perigee rotation were derived and demonstrated by simu-

lation. If the orbit design allows the freedom to choose either the inclination difference or eccentricity difference, then either the differential nodal precession or the differential argument of perigee rotation can be negated. Using these constraints will reduce the amount of fuel required to maintain the formation. The types of formations that can be obtained based on using one, two or three constraints were identified.

Thirdly, the effect of an energy difference on formation design was addressed. It was shown that in contrast to the spherical-Earth problem, equal energy does not prevent drift, except for the case $\delta a = \delta e = \delta i = 0$.

Finally, a method for evaluating modeling error effects for formations has been presented. Results using the method have been presented for a specific PCO or its equivalent for eccentric chief orbits, for a range of eccentricities and formation sizes. For formations that involve out-of-plane motion caused by an inclination difference, one can conclude that not including the chief eccentricity and first-order J_2 effects has a significant effect on predicting relative motion and will waste fuel. The nonlinear effects do not become significant until the formation size is 30–40 km if curvilinear coordinates are used, as is done with the small e theory, the GA theory and the unit sphere nonlinear theory. The Yan–Alfriend theory uses orbital elements.

Analysis of the solutions to the motion variables for near-circular reference orbits showed that unlike for the two-body problem, the fundamental in-plane and cross-track frequencies of perturbed relative motion are in general not the same. A special inclination-phase angle relationship was obtained for which the in-plane and out-of-plane fundamental frequencies are equal, over an extended period of time. Such relative orbits do not precess and, under further restrictions, do not distort in the presence of differential nodal precession. Special values of the orbit inclination were identified for minimizing control requirements for individual satellites as well as a formation. An intelligent control methodology for formation maintenance and inter-satellite fuel-balancing was also presented and the advantage gained by not utilizing radial thrust for formation maintenance near circular orbits was highlighted. This control concept will be validated further in Chapter 10, via detailed numerical simulations using the nonlinear models of relative motion. Mitigating the effects of differential perturbations without the use of thrust involves pitting one disturbance against the other.

Even though the discussion presented in this chapter centered on accommodating J_2 by suitable choices of the initial conditions, other approaches to perturbation mitigation are also possible. For example, Williams and Wang [157] show that secular effects of oblateness can be countered by differential solar radiation pressure for dissimilar satellites in a formation.